

The origin and evolution of fast and slow rotators in the Illustris simulation

Zephyr Penoyre,^{1,2*} Benjamin P. Moster,^{1,3,4} Debora Sijacki¹ and Shy Genel^{2,5}

¹*Institute of Astronomy and Kavli Institute for Cosmology, University of Cambridge, Madingley Road, Cambridge CB3 0HA, UK*

²*Department of Astronomy, Columbia University, New York, NY 10027, USA*

³*Universitäts-Sternwarte, Ludwigs-Maximilians-Universität München, Scheinerstr. 1, D-81679 München, Germany*

⁴*Max-Planck-Institut für Astrophysik, Karl-Schwarzschild Straße 1, D-85748 Garching, Germany*

⁵*Center for Computational Astrophysics, Flatiron Institute, 162 Fifth Avenue, New York, NY 10010, USA*

Accepted 2017 March 24. Received 2017 March 1

ABSTRACT

Using the Illustris simulation, we follow thousands of elliptical galaxies back in time to identify how the dichotomy between fast- and slow-rotating ellipticals (FRs and SRs) develops. Comparing to the ATLAS^{3D} survey, we show that Illustris reproduces similar elliptical galaxy rotation properties, quantified by the degree of ordered rotation, λ_R . There is a clear segregation between low-mass ($M_* < 10^{11} M_\odot$) ellipticals, which form a smooth distribution of FRs, and high-mass galaxies ($M_* > 10^{11.5} M_\odot$), which are mostly SRs, in agreement with observations. We find that SRs are very gas poor, metal rich and red in colour, while FRs are generally more gas rich and still star forming. We suggest that ellipticals begin naturally as FRs and, as they grow in mass, lose their spin and become SRs. While at $z = 1$, the progenitors of SRs and FRs are nearly indistinguishable, their merger and star formation histories differ thereafter. We find that major mergers tend to disrupt galaxy spin, though in rare cases can lead to a spin-up. No major difference is found between the effects of gas-rich and gas-poor mergers, and the number of minor mergers seems to have little correlation with galaxy spin. In between major mergers, lower mass ellipticals, which are mostly gas rich, tend to recover their spin by accreting gas and stars. For galaxies with M_* above $\sim 10^{11} M_\odot$, this trend reverses; galaxies only retain or steadily lose their spin. More frequent mergers, accompanied by an inability to regain spin, lead massive ellipticals to lose most of ordered rotation and transition from FRs to SRs.

Key words: methods: numerical – galaxies: elliptical and lenticular, cD – galaxies: evolution – galaxies: kinematics and dynamics – galaxies: structure.

1 INTRODUCTION

Observed elliptical galaxies may be classified into two groups with respect to their internal properties (Davies et al. 1983; Bender 1988; Bender & Nieto 1990; Kormendy & Bender 1996, 2012). Low- and intermediate-mass elliptical galaxies typically have power-law surface brightness profiles (Lauer et al. 1995; Faber et al. 1997), show little or no radio and X-ray emission from hot gas (Bender et al. 1989), tend to have discy isophotes (Bender, Doebereiner & Moellenhoff 1988; Bender et al. 1989) and exhibit significant rotation along the photometric major axis (Cappellari et al. 2007; Emsellem et al. 2007). On the other hand, massive ellipticals tend to have flat cores, hot gaseous haloes with strong radio and X-ray emission, and box-shaped isophotes. Kinematically they also differ strongly and experience slow rotation, exhibit kinematically decou-

pled components, and have a large amount of minor-axis rotation. The ATLAS^{3D} survey (Cappellari et al. 2011; Emsellem et al. 2011; Krajnovic et al. 2011), which provides a comprehensive view of the properties of a volume-limited sample of local early-type galaxies (ETGs), finds that only a minority of ellipticals fall into the second category. These have also been observed in the Virgo cluster (Boselli et al. 2014). A detailed summary of the properties of elliptical galaxies can be found in Kormendy et al. (2009) and Kormendy (2016).

The dichotomy of the physical properties between the two classes of elliptical galaxies led to the idea that they have different formation histories and form through different mechanisms. Early Λ CDM studies proposed that galaxy properties such as their isophotal shapes and rotation are determined by the angular momentum of infalling gas and the amount of turbulent viscosity (Partridge & Peebles 1967; Larson 1969). In this picture, slow rotators form in rapidly collapsing systems with efficient star formation and gas heating, while fast rotators form in more settled systems in which

* E-mail: zephyrpenoyre@gmail.com

star formation and heating are inefficient. According to an alternative scenario, the ‘merger hypothesis’ (Toomre & Toomre 1972; Toomre 1977), elliptical galaxies form through the morphological transformation of disc galaxies in major mergers, and the properties of the remnants depend on the details of the mergers, such as the mass ratio of the galaxies, the amount of gas in the progenitor discs and their orientation with respect to the orbital plane. This picture became very appealing at the advent of modern hierarchical cosmological models, in which mergers are an important component in the formation and evolution of dark matter (DM) haloes and galaxies (White 1979; Fall & Efstathiou 1980; Davis et al. 1985). Large samples of recent merger remnants are found in the local Universe (e.g. Schweizer 1982; Ellison et al. 2013), and a typical M_* galaxy has experienced a major merger since $z \sim 3$ (Bridge et al. 2007; Tasca et al. 2014).

Consequently, many studies have focused on numerical simulations of isolated, binary galaxy mergers and the properties of the merger remnants (Gerhard 1981; Negroponte & White 1983; Barnes 1988; Hernquist 1993). In recent years, this has led to large libraries of merger simulations, considering both different initial conditions and different feedback schemes (e.g. Cox et al. 2006; Naab, Jesseit & Burkert 2006a; Robertson et al. 2006). While collisionless simulations of major mergers between elliptical progenitors were shown to be in conflict with the observed properties of slow rotators (White 1979; Bois et al. 2010), collisionless simulations of disc galaxies were more successful in reproducing elliptical-like properties. It was demonstrated that the mass ratio has a significant impact on the morphological and kinematic properties of the remnant: major merger simulations lead to slowly rotating, pressure-supported, anisotropic remnants (Negroponte & White 1983; Barnes 1988), while more unequal mass ratios lead to more flattened faster rotating ellipticals with more discy isophotes (Barnes 1998; Naab, Burkert & Hernquist 1999; Bendo & Barnes 2000; Naab & Burkert 2003). However, remnants of gas-poor disc galaxies are in conflict with observations, as they do not reproduce the steep inner profiles. As according to Liouville’s theorem, phase-space density is conserved during a collisionless process, the high central phase-space densities of elliptical galaxies cannot be produced from low phase-space density disc galaxies (Carlberg 1986). In dissipationless simulations, this discrepancy could only be avoided by including large bulge components in the progenitors (Hernquist 1993; Naab et al. 2006a).

A different possibility to solve this problem is to take into account the gas component in the progenitors. During a merger, the gas is torqued and loses its angular momentum driving it to the central regions and increasing the phase-space density (Lake 1989). The presence of gas thus leads to more centrally concentrated remnants with rounder and less boxy centres (Barnes & Hernquist 1996; Bekki & Shioya 1997; Hopkins et al. 2008). Using simulations of binary major mergers, Cox et al. (2006) confirmed that slowly rotating anisotropic remnants can be formed when no gas is present. They also showed that if a cold gaseous component is included in the progenitor discs, some merger orbits lead to fast-rotating remnants, which reproduce the observed distribution of properties of ellipticals. However, the gas fractions that had to be used were relatively high, and only a fraction of merger orbits produced fast rotators, so that it remained unclear whether this scenario can lead to the large number of observed fast-rotating ellipticals. Including a hot gaseous component in the halo, Moster et al. (2011) showed that fast rotators can be formed for most orbits, even if the amount of cold gas in the progenitors is relatively low. As gas subsequently cools from the hot halo and refuels the

cold gas disc, the initial amount of cold gas in the progenitors can be lower. In massive haloes, the hot gas is prevented from cooling by feedback processes, such that more massive systems undergo gas-poor mergers and become slow rotators, while low- to intermediate-mass systems undergo gas-rich mergers and become fast rotators. On the other hand, some studies have argued that fast rotators are created in minor mergers with varying mass ratio (Jesseit et al. 2007, 2009; Bois et al. 2011).

Although binary galaxy mergers have provided many insights into the formation of fast and slow rotators, this approach has significant limitations. The assembly histories of DM haloes and consequently galaxies are considerably more complex than simple binary mergers or sequences thereof. While early growth is dominated by the accretion of gas and subsequent star formation, major and numerous minor mergers with a large range of mass ratios play a significant role in their mass growth (De Lucia & Blaizot 2007; Moster, Naab & White 2013). Moreover, Moster, Macciò & Somerville (2014) showed that multiple mergers, where a second satellite galaxy enters the main halo before the first satellite has merged with the central galaxy, are more common than sequences of isolated binary mergers. It is therefore not possible to simply string the results from binary merger simulations together, but events with three or more galaxies involved have to be considered, which can only be achieved with full cosmological simulations. Using high-resolution cosmological zoom-in simulations, such as Naab et al. (2014, hereafter **N+14**) and Choi & Yi (2017) the formation histories of slow and fast rotators can be studied in a cosmological context. They found that fast rotators are formed when the galaxies have late assembly histories, and that both gas-rich major and minor merger scenarios are common. However, they also identified fast-rotating merger remnants that have formed in gas-poor major mergers of fast-rotating progenitors. Slow rotators can also be formed in various scenarios: either by major mergers (both gas-rich and gas-poor) or by gas-poor minor mergers. While cosmological zoom-in simulations provide a much more detailed view into the different formation mechanisms of slow and fast rotators, they share a significant limitation with binary merger simulations. As the initial conditions (i.e. the systems to be re-simulated) are chosen rather arbitrarily, they do not form a representative sample of local ETGs. This can only be achieved with a volume-limited sample.

In the last years, the field of hydrodynamical simulations of galaxy formation has made large advancements. Modern hydrodynamical codes produce very good results in standard hydrodynamical tests such as fluid instabilities, turbulence and shocks (Teyssier 2002; Springel 2010; Sijacki et al. 2012; Bryan et al. 2014; Hu et al. 2014; Hopkins 2015). Moreover, state-of-the-art feedback methods are able to reduce the baryon conversion efficiency significantly, such that the stellar masses of the simulated galaxies are in good agreement with empirical constraints (Behroozi, Conroy & Wechsler 2010; Guo et al. 2010; Moster et al. 2010). Several studies have now used these powerful codes to run hydrodynamical simulations of cosmological volumes producing galaxy populations that are in good agreement with many observational constraints, such as the stellar mass function, star formation rates (SFRs) and galaxy sizes. Amongst the most detailed simulations are the Magneticum simulation (Hirschmann et al. 2014; Remus et al. 2017), the Illustris simulation (Genel et al. 2014; Vogelsberger et al. 2014), the Horizon-AGN simulation (Dubois et al. 2014; Welker et al. 2014), the MassiveBlack-II simulation (Tenneti et al. 2014; Khandai et al. 2015) and the Eagle simulation (Crain et al. 2015; Schaye et al. 2015). As these simulations trace the formation of galaxies in

a cosmological context for a representative sample of galaxies, they are ideally suited to study morphological and kinematical properties in a statistical manner.

The aim of this paper is twofold: first, we analyse the morphological and kinematical properties of galaxies in the Illustris simulation and compare them to the ATLAS^{3D} observations to judge if the simulated galaxies are a good representation of observed slow and fast rotators. Secondly, we trace the simulated galaxies through cosmic time and investigate which formation channels are the most important ones in the formation of slow- and fast-rotating ellipticals.

The paper is organized as follows. In Section 2, we provide a brief summary of the Illustris simulation. We also explain how we analyse the simulated galaxies and the mergers. In Section 3, we present our results for the slow and fast rotators at $z = 0$ and compare them to the observed sample, including their kinematic properties, the central profiles, the isophotal shapes and the X-ray luminosities. We further present the dependence of the kinematic properties on various galaxy properties, such as their stellar mass, gas fraction, SFR, metallicity, size and colour. In Section 4, we investigate the merger histories of slow and fast rotators, and identify which channels are the most important ones in their formation. Finally, in Section 5, we summarize and discuss our results and compare them to previous studies. Throughout this paper, we assume a 9-year *Wilkinson Microwave Anisotropy Probe* (WMAP9; Hinshaw et al. 2013) Λ cold dark matter (Λ CDM) cosmology with $\Omega_m = 0.2726$, $\Omega_\Lambda = 0.7274$, $\Omega_b = 0.0456$, $h = 0.704$, $n = 0.963$ and $\sigma_8 = 0.809$, and we employ a Chabrier (2003) initial mass function (IMF).

2 METHODS

2.1 The Illustris simulation

Starting with a box of 106.5 Mpc (comoving) on a side, the Illustris simulation tracks DM and baryonic matter in a standard Λ CDM cosmology consistent with the WMAP9 data release (Hinshaw et al. 2013). The simulation is performed using the moving mesh code AREPO (Springel 2010) solving hydrodynamics in a quasi-Lagrangian way, taking advantage of the Voronoi tessellation. For this work, we will focus solely on the largest and best resolved of a suite of simulations, Illustris-1, from now on just referred to as Illustris, following 1820³ DM particles and approximately as many gas elements, with masses and gravitational softening of $m_{\text{DM}} = 6.26 \times 10^6 M_\odot$, $m_{\text{gas}} = 1.26 \times 10^6 M_\odot$, $\epsilon_{\text{DM}} = 1.42$ kpc and $\epsilon_{\text{gas}} = 0.71$ kpc, respectively. For further details of the simulations, see Vogelsberger et al. (2014) and Genel et al. (2014).

In addition to gravity and hydrodynamics in an expanding universe with a uniform ionizing background, a suite of sub-grid models are used that are crucial to galaxy formation and evolution. Radiative heating and cooling processes including both primordial and metal-line cooling are incorporated and high-density gas can cool to form star particles. These have their own associated IMF, return mass and metals in accord with the stellar evolutionary tracks and produce corresponding feedback through supernovae, leading to galactic-scale winds. A simple recipe for the formation of massive seed black holes is adopted, motivated by the direct collapse scenario. Black holes then can grow through accretion and mergers, and AGN feedback including quasar, radio and radiative modes is modelled (Sijacki et al. 2015). The free parameters of these sub-grid models are tuned to reproduce the $z = 0$ stellar mass function, cosmic SFR evolution and the mass–metallicity relation. Vogelsberger et al. (2013) present full details of the methods employed and how the free parameters are set.

A total of 136 snapshots are taken at particular redshifts, spaced for the later part of the simulation since $z = 3$ by $\Delta a \approx 0.01$, where a is the cosmological scalefactor. Together with the data stored in the snapshots, the on-the-fly friends-of-friends and SUBFIND algorithms (Springel, Yoshida & White 2001; Dolag et al. 2009) provide catalogues of virialized DM haloes and their bound subhaloes, including a number of their properties. For further details, see the public release paper (Nelson et al. 2015).

At $z = 0$, there are 4366 546 gravitationally bound subhaloes. 309 166 of these subhaloes contain star particles, and henceforth we call these galaxies. We define, in Section 2.3, the limit of a well resolvable galaxy to be one with over 20 000 star particles and at $z = 0$ we find 4591 qualifying galaxies in the Illustris simulation, including satellite galaxies as well as centrals. Taking advantage of the merger trees constructed following Rodriguez-Gomez et al. (2015), we can trace back in time the identity and properties of the progenitor galaxies, and by combining this information with subhalo and particle catalogues analyse the nature and effect of galaxy mergers and the evolution of galactic properties over cosmic time.

2.2 Modelling galaxies via stellar kinematics

As we will be comparing to observational data, all our kinematic analysis is based almost solely on the motions of star particles, ignoring black holes, DM and gas. We also work directly with the mass of each star particle, which means that where we compare to observational measures that examine a galaxy’s light profile we make the implicit assumption of a constant mass-to-light ratio.

To find the centre of the galaxy, we take the position of the most bound star particle. We determine the galaxy’s velocity via the centre of mass velocity of the most bound 50 per cent of particles; this avoids substructure at large radii with high velocities biasing the result. We also exclude stars outside of 50 kpc (comoving) of the centre, which aids in the exclusion of satellites at large radii, particularly a problem for the highest mass galaxies. In the rest frame centred on the galaxy, each star particle denoted with index i has a position r_i , velocity v_i and mass m_i . We hence calculate the specific angular momentum of each star particle j_i and to find the plane of the galaxy we use the total angular momentum of the most bound 50 per cent of particles, \hat{J} .

2.3 Classifying spirals and ellipticals

We limit our sample only to elliptical galaxies, and hence must cut any spirals from our sample. This is easy enough to do via visual examination when having a small sample, but it is unfeasible for such a large sample as we have from Illustris. Instead, we use the method outlined in Sales et al. (2012, hereafter S+12) to compute the κ parameter, which measures the fraction of kinetic energy invested in ordered rotation, i.e.

$$\kappa = \frac{K_{\text{rot}}}{K}, \quad K_{\text{rot}} = \sum \frac{1}{2} m_i \left(\frac{j_{z,i}}{R_i} \right)^2, \quad (1)$$

where K_{rot} is the total kinetic energy invested in ordered rotation, dependent on the particle’s mass, cylindrical radius $R_i = (r_i^2 - (\mathbf{r}_i \cdot \hat{J})^2)^{1/2}$ and specific angular momentum perpendicular to the disc $j_{z,i} = \mathbf{j}_i \cdot \hat{J}$. K is the total kinetic energy of the galaxy, and both measures of kinetic energy are calculated over all star particles.

For a perfectly rotating, completely disc-dominated galaxy κ will tend to 1, whereas for a bulge-dominated or elliptical galaxy κ will tend to 1/3. We define the cutoff between elliptical galaxies

and spiral galaxies to be $\kappa = 0.5$, which gives a realistic ratio of galaxies at high masses. These cuts are in good agreement with observations (Conselice 2006) for all large galaxies. However, for galaxies with $M_* \lesssim 10^{10.5} M_\odot$, we start to see unexpectedly high fractions of ellipticals. We present these results, as well as a discussion of other possible methods to separate the populations, in Appendix A.

Similar results were seen in Illustris by Snyder et al. (2015) and Rodriguez-Gomez et al. (2017), where low-mass galaxies are bulge dominated by kinematic measures, but have SFRs and disc properties characteristic of spiral galaxies. The conclusion that we draw from this is that low-mass galaxies in Illustris, with less than $\sim 10^4$ star particles, cannot be satisfactorily examined on a kinematic basis. This could be due to deficiencies in the feedback mechanisms that are needed to create an extended disc in simulation, and/or the poor resolution of these low-mass galaxies. We thus draw a line between galaxies that can reasonably be resolved and kinematically classified and those that cannot. From now onwards, we will restrict our analysis to galaxies with over 20 000 star particles, roughly corresponding to a stellar mass of $10^{10.5} M_\odot$.

2.4 Examining galaxies in projection

To compare with observational data, we must project our three-dimensional galaxy data on to a two-dimensional image seen from a particular line of sight. We can choose an arbitrary, fixed, line of sight throughout and thus our results will be statistically comparable to observable data, or we can rotate each galaxy such that we observe it edge-on allowing us to take intrinsic values of shape and motion. We will do both in the course of this analysis to examine the effects of projection on our data set.

When using an arbitrary line of sight, we choose to look directly along the z -axis, such that line-of-sight velocity $V_i = v_{z,i}$ and two-dimensional projected position $\mathbf{R}_i = r_{x,i} \hat{\mathbf{i}} + r_{y,i} \hat{\mathbf{j}}$. To gauge the intrinsic properties of galaxies, we use the inertia tensor (see e.g. Joachimi et al. 2013),

$$I_{\mu,\nu} = \frac{\sum m_i r_{\mu,i} r_{\nu,i}}{\sum m_i} \quad (2)$$

(where the sum is performed over the 50 per cent most bound star particles), to project the galaxy so as to extremize its ellipticities. From the eigenvectors of \mathbf{I} , \mathbf{e}_1 , \mathbf{e}_2 and \mathbf{e}_3 (corresponding to the long, medium and short axes of the approximated ellipsoid, respectively), we find the projected line-of-sight velocities $V_i = \mathbf{v}_i \cdot \mathbf{e}_2$ and two-dimensional projected positions $\mathbf{R}_i = (\mathbf{e}_1 \cdot \mathbf{r}_i) \hat{\mathbf{i}} + (\mathbf{e}_3 \cdot \mathbf{r}_i) \hat{\mathbf{j}}$.

We find the projected circular stellar half-mass radius, r_h , and then make a grid of 48 by 48 square pixels, scaled initially to make an image $4 r_h$ wide, centred on the galaxy. The grid can be dynamically resized to ensure that all relevant data are included at the highest possible resolution, though the factor of 4 is chosen to ensure that this is rarely necessary.

Using the projected positions of each star particle, \mathbf{R}_i , we create 20 pseudo-particles, each with $\frac{1}{20}$ th the original mass, and randomly distribute them around the original projected position with displacements drawn from a two-dimensional Gaussian with a standard deviation of 0.3 kpc, from which we determine which, if any, pixel they reside in. Each pixel, which we label n of $N (= 48 \times 48 = 2304)$, now contains I_n star pseudo-particles, which in turn we index using i_n , corresponding to the subset of indices of star particles i contained in pixel n . We then find the total mass of stars projected in each pixel M_n , their centre of mass line-of-sight velocity V_n and the mass-weighted dispersion in line-of-sight velocity, σ_n , computed

relative to V_n . To further analyse the galaxy, we then examine a contour of pixels that contains half the galaxy's mass. It is from this subset of pixels that we analyse the rotation properties of the galaxy, and from the outline of this contour that we measure the galaxy's shape.

In finding this contour, we use a novel approach. Starting from a pixel at the centre of our image, we sequentially add the next heaviest pixel adjacent to any of the pixels already included. We continue to add pixels in this manner, filling any internal gaps when they arise, until the total mass of the pixels contained has exceeded half the total mass of the galaxy. This method creates a single connected contour that well represents the shape of the galaxy's isodensity contour. We then fit an ellipse to the pixels that lie on the edge of this contour to find the semi-major and semi-minor axes, a and b , respectively and thus the ellipticity of the galaxy, ϵ .

We experimented with an alternative expression for ellipticity, as presented in Emsellem et al. (2007), which takes account of the internal structure of the galaxy as well as the external contour

$$\epsilon' = 1 - \sqrt{\frac{\langle x^2 \rangle}{\langle y^2 \rangle}}, \quad (3)$$

where x and y correspond to the components of the projected position vector \mathbf{R}_i and the angular brackets denote the mass-weighted mean of the pixels included in the contour. This was previously used as a flux-weighted mean but with our assumption of constant mass-to-light ratio the two are equivalent.

We found both measures to be in very good agreement, suggesting that the shape of the external contour well represents the internal structure and we have chosen to classify the galaxies in our sample using ϵ rather than ϵ' as this quantity is more readily available to observers.

Finally, we use our projection to find λ_R , the degree of ordered rotation. We have

$$\lambda_R = \frac{\langle R|V| \rangle}{\langle R\sqrt{V^2 + \sigma^2} \rangle}, \quad (4)$$

where $\langle \rangle$ refer to a mass-weighted mean.

For perfectly ordered rotation, we expect the velocities of particles to be much greater than the local velocity dispersion and hence λ_R will tend to 1. In practice, values higher than ~ 0.8 are very rare in elliptical galaxies, perhaps as their past mergers have flung some stars into non-uniform orbits. For the most perturbed galaxies, we expect there to be no clear direction of motion for each pixel and hence the projected velocity dispersion should hugely outweigh any ordered rotation, giving values of λ_R tending to zero.

We applied each of the above analyses to every galaxy with over 20 000 star particles at each snapshot from $z = 4$ to 0, such that we could track the type, shape and degree of rotation of each galaxy back up to 12 billion years ago. Fig. 1 shows an example of our methods for six illustrative elliptical galaxies at $z = 0$. There are three pairs of fast and slow rotators (cutoff criteria are explained in Section 3) at low mass (top, $M_*/M_\odot < 10^{11}$), intermediate mass (middle, $10^{11} < M_*/M_\odot < 10^{11.5}$) and high mass (bottom, $10^{11.5} < M_*/M_\odot$), as indicated in the first column. All are relatively elongated and of similar half-mass radii. As shown in the panels in the second and third columns, the fast rotators show a clear velocity signature, with rotation well aligned from small to large radii, whilst slow rotators are much more disordered with generally lower speeds and comparable or higher velocity dispersions. In the fourth column, we show a visualization of the relative contribution of different parts

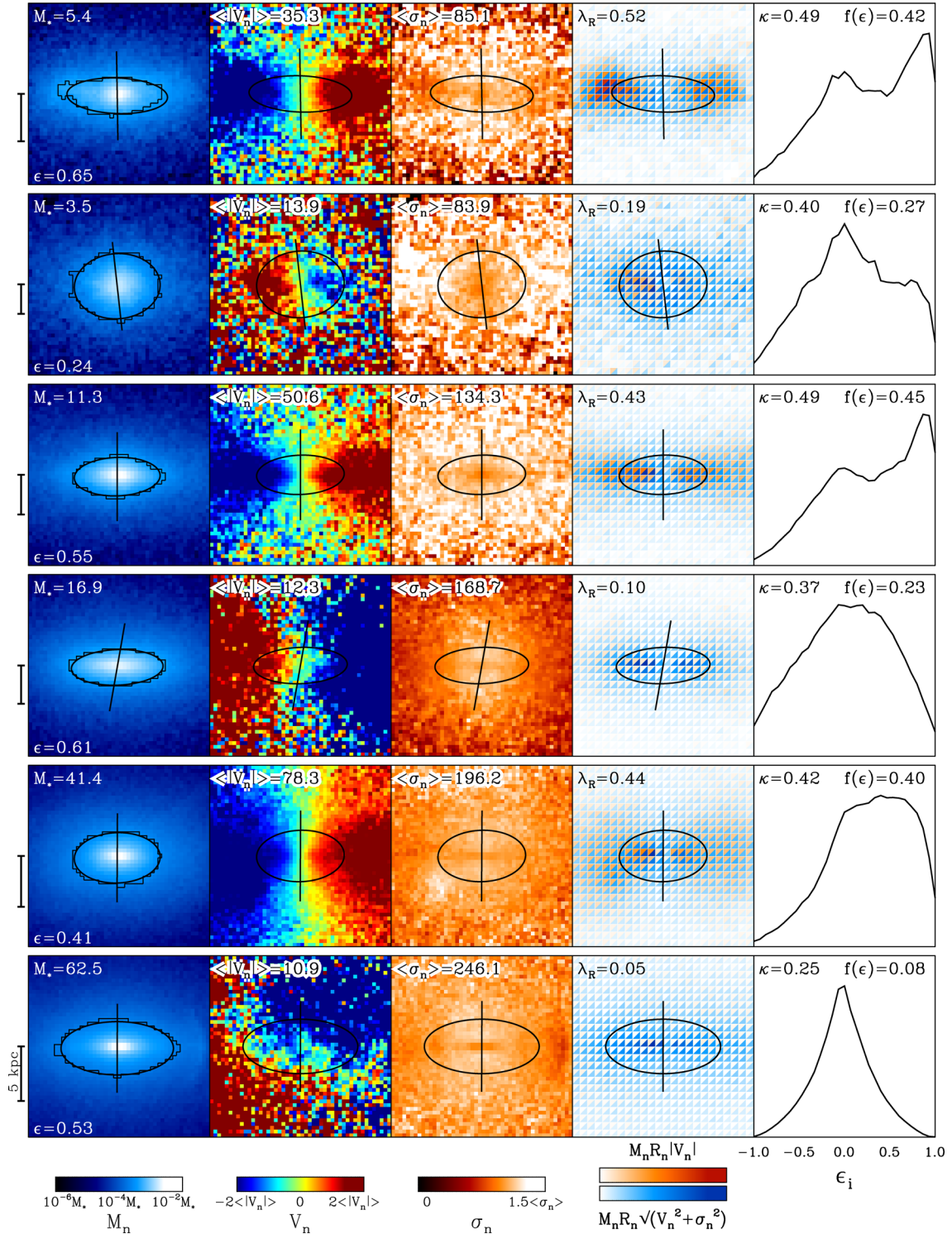


Figure 1. Projected properties of six illustrative elliptical galaxies at $z = 0$, showing in descending order, a low-mass FR and SR, an intermediate-mass FR and SR and finally a high-mass FR and SR. From left to right plots show projected density, line-of-sight velocity, line-of-sight velocity dispersion, contribution of pixels to ordered versus disordered components of λ_R , and finally the distribution of the circularity parameter (as detailed in Appendix A). Each galaxy is projected along the medium axis of the inertia tensor, and plotted with the minor axis in the vertical direction. In the first column, the contour of pixels containing half the galaxy’s mass is shown, to which the ellipse is then fitted. The black line on each galaxy shows the projected direction of the total angular momentum. Scale bars are all 5 kpc long. M_* is the total stellar mass in units of $10^{10} M_\odot$, $\langle v \rangle$ and $\langle \sigma \rangle$ are mass-weighted line-of-sight velocity and velocity dispersion, respectively (in km s^{-1}). λ_R is the degree of ordered rotation and ϵ is the projected ellipticity. κ is the fraction of kinetic energy devoted to circular orbits in the plane and $f(\epsilon)$ is the fraction of stars with a disc-like circularity parameter. The mass and spin histories of these six galaxies are shown and discussed in Fig. 2.

of the galaxy to the numerator and denominator of equation (4) (normalized by the maximum pixel value of either for the galaxy). These show that there is similar structure in the measure of disorder of all galaxies (the denominator) but that fast rotators have a much larger degree of ordered rotation (numerator) corresponding to disc-like rotation and that this continues out to large radii. Finally, in the fifth column, we show the disc–bulge comparison and can see that FRs have significant disc-like components (though not dominant) although towards higher mass the disc and the bulge become difficult to separate.

2.5 Following the merger histories of massive galaxies

We take advantage of the galaxy merger trees to look at the accretion histories of the galaxies in our sample, examining how mergers influence galaxies with different intrinsic properties at $z = 0$. The merger trees are generated using the SubLink algorithm, as detailed in Rodriguez-Gomez et al. (2015). We combine the calculated values of λ_R , ϵ , κ and j with the data stored in the SubLink trees for stellar mass M_* , and gas mass M_g , within two stellar half-mass radii. We follow these properties back in time along the main progenitor branch of each galaxy at $z = 0$.

Following the prescription of Rodriguez-Gomez et al. (2015) for each subhalo that merges with the main progenitor at a particular redshift, we trace that subhalo back to the point at which its stellar mass is maximum, approximately the point at which the galaxies begin tidally interacting, and we record its properties. We classify major mergers as those for which the stellar mass of the merging subhalo, $M_{*,i}$, satisfies $M_{*,i} > \frac{1}{4}M_*$ and all other mergers are classified as minor mergers. Thus, we calculate the total stellar mass accreted at each snapshot through major mergers, $\Delta M_{*,\text{maj}}$, and through minor mergers, $\Delta M_{*,\text{min}}$, and similarly for the gas mass accreted through major, $\Delta M_{g,\text{maj}}$, and minor, $\Delta M_{g,\text{min}}$, mergers.

We find a rough estimate for the change of stellar mass due to *in situ* star formation at some snapshot n as $\Delta M_{*,\text{situ}}(n) = M_*(n) - M_*(n-1) - \Delta M_{*,\text{maj}}(n) - \Delta M_{*,\text{min}}(n)$, i.e. any stellar mass change not accounted for by mergers is assumed to stem from *in situ* star formation. However, as stellar mass is transferred between galaxies throughout a merger, and more galaxies may join the interaction during the infall period, this simple treatment is unlikely to perfectly capture the mass changes (e.g. see Rodriguez-Gomez et al. 2016 for more details). Also, this formulation assumes no mass-loss through stripping or stellar evolution and hence in practice may underestimate the *in situ* star formation for galaxies with violent collisions that fling out a significant mass fraction (and negative values of $\Delta M_{*,\text{situ}}(n)$ are thus possible).

Fig. 2 shows the evolution since $z = 2.5$ of the six galaxies from Fig. 1. There are several interesting features to note. Both of the lower mass galaxies only have λ_R defined for the later part of this period, because before that point they are not categorized as well-resolved ellipticals. All galaxies grow in mass by about an order of magnitude in this period (solid black curves), whilst their gas content stays roughly constant or reduces (solid blue curves). Major mergers (indicated with grey bands) are associated with large changes in their rotation (dashed red curves) and also their angular momentum (not shown here but well correlated with λ_R), but substantial changes can also occur over periods without major mergers. Section 4 details analysis of the histories of the whole population of thousands of well-resolved ellipticals in Illustris.

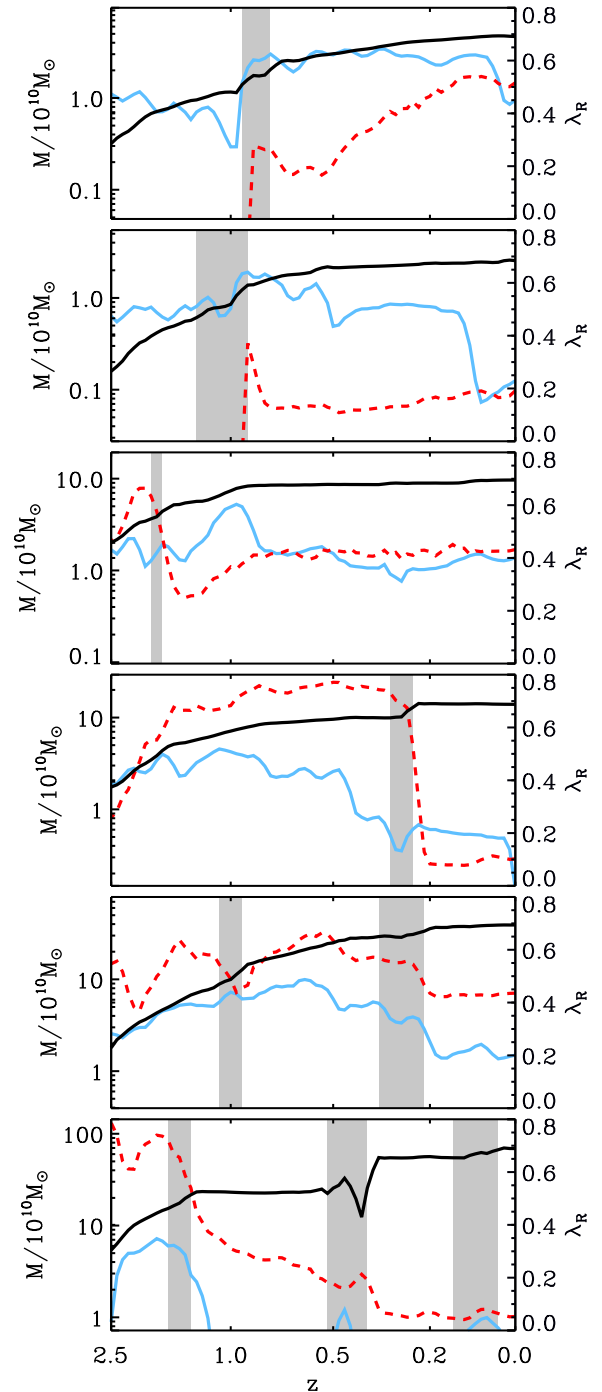


Figure 2. Evolution of the six galaxies shown in Fig. 1 since $z = 2.5$. The solid black line shows the stellar mass, M_* , and the solid blue line the gas mass, M_g , the scale for both is shown on the left. The dashed red line shows the degree of ordered rotation, λ_R , the scale for which is shown on the right. The grey regions are the period in which the galaxy is undergoing a major merger, starting at the point of maximum stellar mass of the incoming body (roughly the start of the encounter). From top to bottom low-mass FR and SR, intermediate-mass FR and SR and high-mass FR and SR are shown.

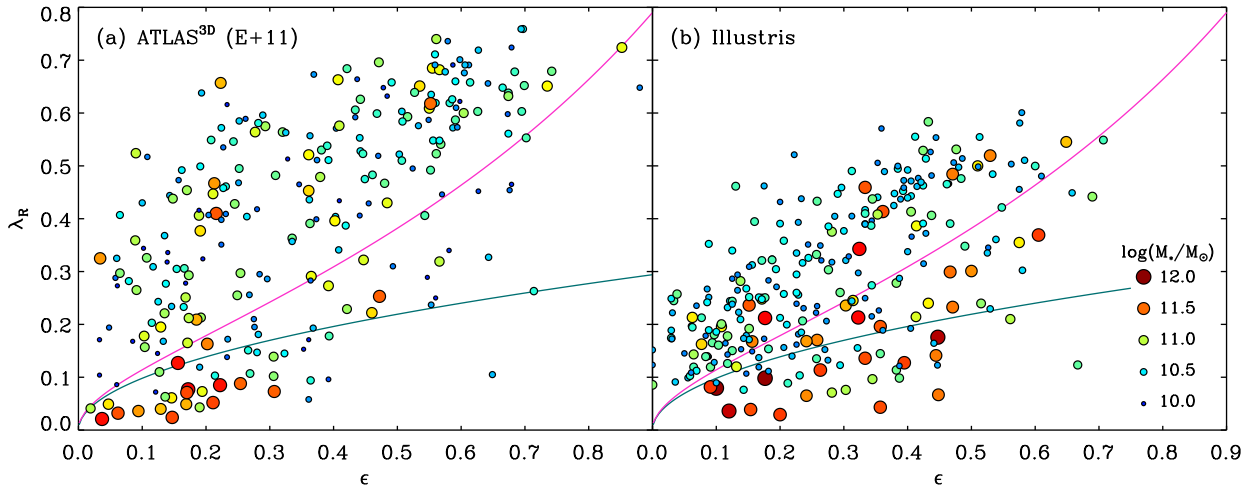


Figure 3. Distribution of ETGs in the ϵ - λ_R plane, (a) reproduced from the ATLAS^{3D} survey (E+11) compared to (b) those created in the Illustris simulation, sampled based on the same selection criteria (see the text for more details). The magenta line shows the line on which edge-on elliptical galaxies with the same degree of rotational support would lie, as described in the text and re-derived in Appendix C. The green line follows equation (5), defining the cutoff below which galaxies are classified as SRs. Each galaxy is represented by a circle whose colour and size scale with the stellar mass.

3 POPULATIONS OF FAST AND SLOW ROTATORS

3.1 Comparing to the ATLAS^{3D} survey

The first question we seek to answer is whether the Illustris simulation produces a representative sample of fast and slow rotators. The ATLAS^{3D} survey provides an excellent set of observational data to compare to Emsellem et al. (2011, hereafter E+11), examining the distribution of ellipticity and λ_R for 260 ETGs in a volume- and magnitude-limited sample. We reproduce their results in the left-hand panel of Fig. 3.

E+11 selected ETGs based on whether they could clearly discern spiral arm structures in the galaxy. Taking into account the variation due to projection effects in observed galaxy properties, E+11 suggested making a divide between FRs and SRs based on their ϵ and λ_R properties using the curve

$$\lambda_{R,\text{cutoff}} = 0.31\sqrt{\epsilon}, \quad (5)$$

above which galaxies are classified as FRs and below as SRs. Of their sample, 224 galaxies, or 86 ± 2 per cent, were classified as FRs and the remaining 36, 14 ± 2 per cent, as SRs, using equation (5) to divide the population.

They found FRs to be roughly oblate, with the ellipticity of a galaxy correlating linearly with its anisotropy, β . In other words, the FRs are roughly rotationally supported with stars on mostly circular orbits. Thus, the motions of stars and the projected shape of the galaxy have a simple, linear correlation. SRs are instead galaxies with low degrees of rotational support, with many stars on radial or generally irregular orbits. Thus, we can identify galaxies whose shape is well represented by the assumption of rotational support, those with ellipticity (ϵ) proportional to their degree of velocity anisotropy (δ). Cappellari et al. (2007) and E+11 find an approximate expression for the variation of λ_R with ϵ for galaxies with $\delta \propto \epsilon$. We detail this expression in Appendix C, and follow their lead in showing the relationship for $\delta = 0.7\epsilon$ as a magenta line in the left-hand panel of Fig. 3.

The E+11 sample of galaxies is volume and magnitude limited to those galaxies within 42 Mpc, brighter than $M_{K_s} = -21.5$ mag, which are clearly visible from the William Herschel Telescope (declination $|\delta - 29^\circ| < 35^\circ$) and which are far from the Galactic plane to avoid contamination (galactic latitude $|b| > 15^\circ$). Using the same criteria (arbitrarily setting the equatorial direction aligned with the positive z -axis and the galactic plane relative to that), we took a sample of galaxies from Illustris, shown in the right-hand panel of Fig. 3, finding 270 galaxies. Of this sample, 38, or 14 per cent, are SRs and 86 per cent FRs.

The number of galaxies and fraction of FRs and SRs are in very good agreement between the ATLAS^{3D} survey and the Illustris simulation. We also find that the majority of FRs are lower mass galaxies whilst the highest mass galaxies are mostly SRs, as found in observations as well. However, there are fewer high- λ_R galaxies than the ATLAS^{3D}. This may be a selection effect, as in the ATLAS^{3D} survey ETGs are selected by excluding any galaxies with visible spiral arms. Thus, it is possible that some fast-spinning disc-like objects, with no clearly visible spiral arms, are included. Our elliptical galaxies are selected by comparing the fractional energy in the disc and the bulge, thus excluding the fastest rotating and most disc-like structures. It could also suggest, as we discuss in Section 2.3, that there may be limitations to the simulation at producing extended rotationally supported low-mass objects.

Simulated high-mass SRs show higher ellipticities than we might expect. We believe that this may be due to the specific sub-grid physics choices of the Illustris simulation, particularly due to the role of gas in major mergers. It has been shown that the presence of a high gas fraction can lead to a more rounded slow-rotating galaxy, as in Jesseit et al. (2007, 2009) and N+14, and that the success in reproducing observed kinematics from major mergers is strongly dependent on the gas component for SRs, though FRs are not as affected (Bois et al. 2010).

This tendency to slower spinning, more rounded observed galaxies shows the limitation of the simulation's ability to capture the full detail of these galaxies, but the very good overall qualitative and quantitative agreement leads us to conclude that the Illustris

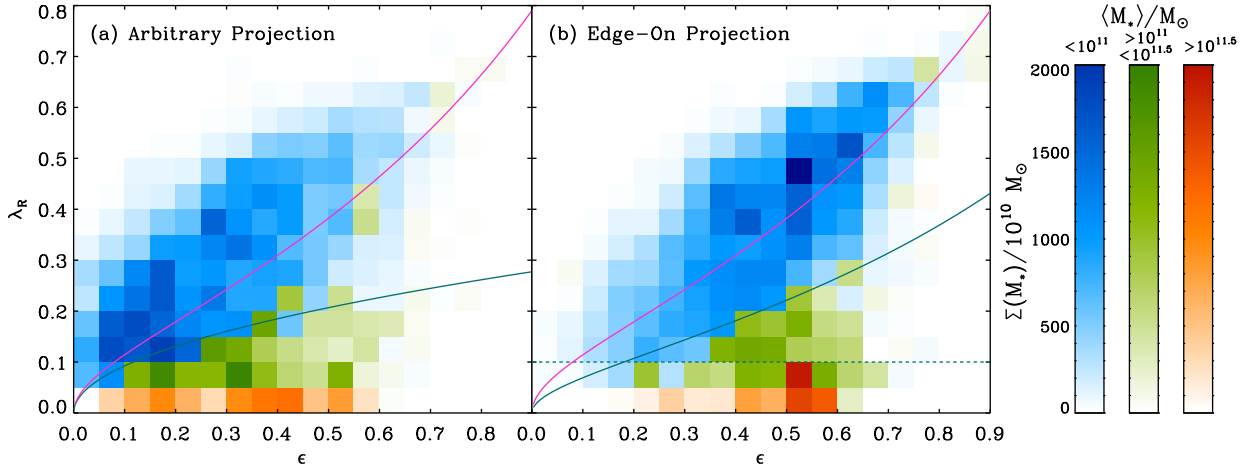


Figure 4. Left-hand panel (a): properties of galaxies when viewed from an arbitrary projection angle, shown for every elliptical galaxy between $z = 0.1$ and 0. Right-hand panel (b): similar figure for edge-on projections of each galaxy between $z = 0.1$ and 0. The colour of pixels is defined by the average mass of the galaxies contained and its colour saturation by the total mass of the galaxies contained in that pixel (normalized compared to highest total mass pixel). The solid green lines refer to the FR–SR cutoff for both projections. The dotted green line shows the previously suggested cutoff of a fixed value of λ_R (see the text for more details).

galaxies comprise a sufficiently representative sample of fast- and slow-rotating galaxies on which to base the analysis that will follow.

3.2 Simulated FR and SR populations for a larger sample

By including the whole population of well-resolved elliptical galaxies and considering multiple snapshots, we create a large sample of galaxies from which distributions of galaxy properties can be derived. Starting from our arbitrary line of sight, we analyse λ_R and ϵ for 15 774 elliptical galaxies with over 20 000 star particles each. Of these, 86.8 per cent are classified as FRs and 13.2 per cent as SRs.

For this large population sample between $z = 0.1$ and 0, the left-hand panel of Fig. 4 shows similar characteristics to the subsets shown in Fig. 3, with a clear segregation based on the mass of a galaxy. More massive galaxies tend to have low values of λ_R and are classified as SRs, while the lower mass galaxies form the bulk of FRs, the majority of which reside above and to the left of the magenta line, showing significant rotational support. Note that there is a particularly high number of FRs concentrated around $(\epsilon, \lambda_R) \approx (0.1, 0.15)$. Intermediate-mass galaxies with $10^{11} M_\odot \leq M_* \leq 10^{11.5} M_\odot$ occupy the region in between and are classified as a mixture of FRs and SRs.

We also present results for galaxies projected edge-on, allowing us to gauge their intrinsic properties, as shown in the right-hand panel of Fig. 4. Of 15 774 galaxies, 95.7 per cent are FRs and 4.3 per cent are SRs, based on the previously suggested cutoff for the intrinsic spin of galaxies of $\lambda_R = 0.1$ (J+09). We suggest an improvement to this simplistic cutoff between FRs and SRs. We use a linear scaling of the line defining galaxies with a constant degree of rotational support, with a constant of proportionality chosen to recover similar fractions of SRs and FRs as found for an arbitrary projection angle. We thus use the approximate relation shown as the magenta line in Fig. 3 (the form of which is reproduced in Appendix C), i.e.

$$\lambda_{R,\text{cutoff}} = \alpha \lambda_R \text{ for } \delta = 0.7\epsilon \quad (6)$$

for some constant α . For $\alpha = 0.65$, we find 86.6 per cent FRs and 13.4 per cent SRs. We also find good agreement between whether any individual galaxy is classified as an SR in an arbitrary projection

and an edge-on projection, with over 90 per cent overlap for more massive galaxies (~ 75 per cent for low mass). Comparing the fraction of FRs predicted by this cutoff with those found for galaxies projected along an arbitrary line of sight, we see very good agreement. It should be noted that the chosen value of $\alpha = 0.65$ is left purposefully imprecise as the cutoff line is not strongly physically motivated and thus is at best a useful rough approximation. Fine-tuning of α can give an even tighter correlation but also a misleading impression of the precision of the cutoff criteria.

Examining the two panels in Fig. 4, we see that many galaxies have shifted towards higher ϵ and λ_R , in agreement with the expectation that these values are maximal when viewed edge-on. We see, as before, a clear distinction between the majority of FRs being lower mass galaxies and the majority of SRs being intermediate and higher mass galaxies, with the most massive galaxies dominating at the lowest values of λ_R .

3.3 Kinematic properties of galaxies as a function of their mass

Our divisions between low-, intermediate- and high-mass galaxies ($M_*/M_\odot < 10^{11}$, $10^{11} \leq M_*/M_\odot < 10^{11.5}$ and $10^{11.5} < M_*/M_\odot$, respectively) whilst set quite arbitrarily, actually serve to provide strongly contrasting trends in their kinematics at $z = 0$. In Fig. 5, we present the edge-on distributions of populations of low-, intermediate- and high-mass galaxies independently, which together make up all the resolvable galaxies in the interval from $z = 0.1$ to 0.

Starting with the low-mass bracket, we now see a very clear locus of points around which these galaxies are clustered along a line roughly parallel with equation (C5) passing through the point $(\epsilon, \lambda_R) \approx (0.5, 0.5)$. Though some low-mass galaxies cross the FR–SR boundary, these do not seem to be a separate population, just a natural spread in the distribution. This may suggest that low-mass galaxies classified as SRs are not in fact part of a separate population from low-mass FRs; they are the tail end of the FR distribution.

Next examining the highest mass range, we see a clear tendency to low λ_R values, with the majority being classified as SRs. There is a much more scatter, due to the lower numbers of higher mass galaxies, but the galaxies seem to be roughly clustered around a

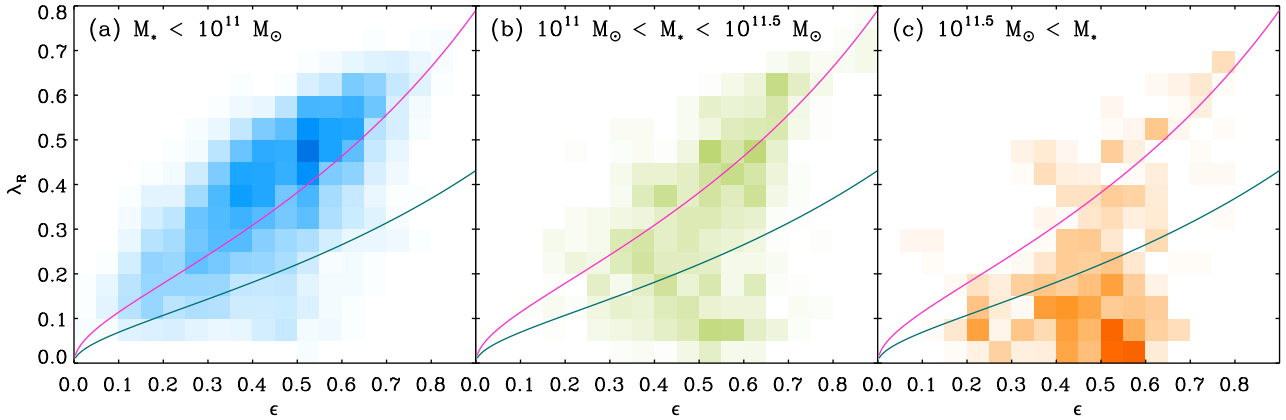


Figure 5. Intrinsic ϵ - λ_R plots as in previous figures, now separated by galaxy mass. From left to right low-mass ($<10^{11} M_\odot$), intermediate-mass (between 10^{11} and $10^{11.5} M_\odot$) and high-mass ($>10^{11.5} M_\odot$) galaxies are plotted. Note the clear distinction between the regions occupied by low- and high-mass galaxies, which could explain the observed distinct populations of fast- and slow-rotating galaxies.

point at $(\epsilon, \lambda_R) \approx (0.55, 0.05)$. It is worth noting that there also exist some high-mass galaxies with high λ_R values, which could either be the high-mass tail of the lower mass galaxy distribution or could be galaxies spun up by a fortunate major merger (whilst we expect the majority of major mergers to cause spin-down, see Section 4.4).

The boundaries for the intermediate-mass bracket have been picked rather arbitrarily, but seem to well separate two regions with much more pronounced properties, and intermediate-mass galaxies themselves seem to broadly fall into one of these two groupings.

We also examined the distribution of galaxy morphologies for the central galaxies (corresponding to the primary DM haloes) compared to satellite galaxies and find that both seem to follow the same distributions in (ϵ, λ_R) space, a trend that has since been observed in the MaNGA survey (Greene et al., in preparation). This suggests that environmental effects, on the scale of individual DM haloes, do not have a large impact on spin properties.

The sharp distinction between the low- and high-mass galaxies, as seen in Fig. 5, and their correspondingly discrete distributions of λ_R are striking, and could feasibly explain the observed distinct populations of fast- and slow-rotating galaxies.

3.4 Cosmic evolution of SR and FR fractions

In Fig. 6, we show a series of ϵ, λ_R plots for redshift intervals: $0.1 \leq z \leq 0.5$, $0.5 \leq z \leq 1$, $1 \leq z \leq 2$ and $2 \leq z \leq 4$. We observe a decreasing population of high-mass galaxies with increasing z , in accord with the hierarchical galaxy assembly, and of SRs as well, highlighting their dependence on past merger histories. Of those galaxies that are classified as SRs, particularly at higher redshifts, many appear to be part of a natural spread of FRs, as we have previously suggested in Section 3.3 and excluding these we see negligible SR fractions until roughly $z = 1$, in agreement with the establishment of the galaxy red sequence at about this epoch in the Illustris simulation. At all redshifts, FRs still seem to be centred at roughly the same (ϵ, λ_R) .

3.5 Alternative methods for classifying fast and slow rotators

Whilst the λ_R parameter is perhaps the best measure of the kinematic properties of an elliptical galaxy, there are a variety of other properties that separate the population of fast- and slow-rotating ellipticals (see e.g. Kormendy et al. 2009; Kormendy 2016). They

relate to many different properties of these galaxies, from their density profiles to their luminosities, and we summarize here tests of some of these criteria on the massive ellipticals in Illustris.

3.5.1 Cusps versus cores

Slow rotators generally exhibit flattened density profiles at their centres (cores) whilst most fast rotators have rapidly rising density at small radii (cusps). These may be the result of binary supermassive black holes at the centres of galaxies scouring the local stellar population and leading to an evacuated core (Merritt 2006). This would not be realizable by the Illustris simulation, where black hole merging is not followed at small scales due to the spatial resolution limitations.

Due to the gravitational softening length of stellar particles being of the order of 1 kpc, it is impossible to judge whether low-mass galaxies have cuspy density profiles as the scale of a cuspy or cored profile is of the same order as the softening length. For the most massive galaxies, whose cores have characteristic lengths larger than the softening length and so are resolvable, we see cored density profiles. These galaxies are almost all SRs so this is well in line with observations. For galaxies with $M_* > 10^{12} M_\odot$, we see core radii mostly between 3 and 5 kpc.

3.5.2 Boxy versus discy isophotes

Fast-rotating ellipticals, with a significant fraction of stars still on disc-like orbits, should appear slightly discy when viewed edge-on, with a central bulge and elongated fringes. Conversely, slow rotators are more rounded and less discy, and can even have boxy isophotes, with bulges off-axis (Naab et al. 2007; Mo, van den Bosch & White 2010).

If we fit an ellipse with radius $R_{\text{ell}}(\phi)$ to the isophote with radius $R_{\text{iso}}(\phi)$ and express the residuals as a Fourier series

$$\Delta(\phi) = R_{\text{iso}}(\phi) - R_{\text{ell}}(\phi) = \sum_{n=1}^{\infty} a_n \cos(n\phi) + b_n \sin(n\phi), \quad (7)$$

the sign of the a_4 parameter tells us if the elliptical is boxy ($a_4 < 0$) or discy ($a_4 > 0$).

We perform this analysis for every central galaxy in Illustris at $z = 0$, fitting ellipticals to isodensity contours and fitting Fourier series to the residuals. In Appendix B, we discuss the methods used in more detail, and present a visual example of the success and failures of capturing the contours of a galaxy with this technique.

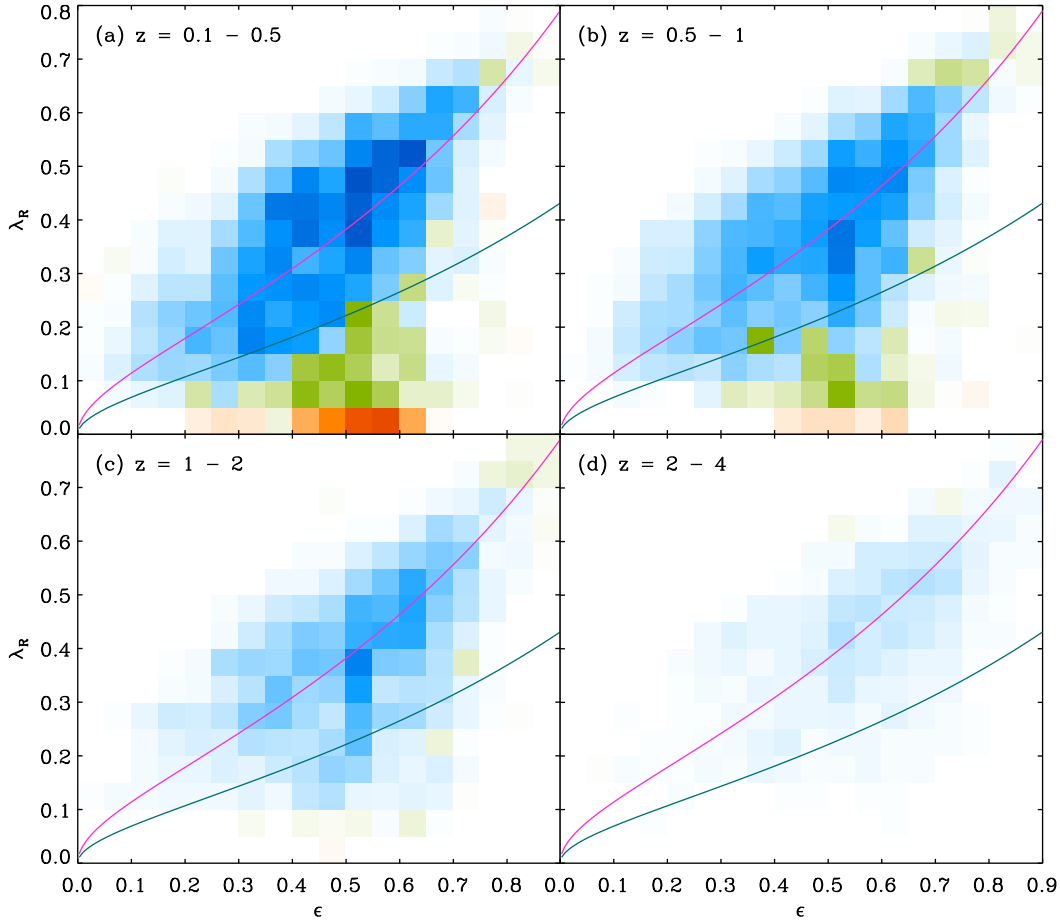


Figure 6. Similar to Fig. 4 showing properties of elliptical galaxies, in edge-on projection, over intervals of redshift going back in time to $z = 4$. While FRs are present at all epochs, SRs exist only for $z < 1$ in agreement with the establishment of the galaxy red sequence in Illustris at about this epoch.

The upper panel of Fig. 7 shows the distribution of boxy and discy FRs and SRs, plotted as pixels for galaxies with $M_* < 10^{11.5} M_\odot$ and as individual points for more massive galaxies. The population of galaxies is similar to the observed ATLAS^{3D} sample (fig. 13 of E+11) and with simulated merger remnants including winds and gaseous haloes (Moster et al. 2011).

The majority of low-mass galaxies are discy FRs, as expected, but with significant variation encompassing some discy SRs and boxy FRs. However, examining the fitting of contours to individual galaxies shows that for these smaller, less well-resolved galaxies the contour fit can be erroneously dominated by small morphological features. Hence, much of this spread of properties may be numerical rather than representative of galaxy properties, as detailed in Appendix B.

Looking at the high-mass galaxies, we see almost no boxy FRs and a high number of discy FRs, as would be expected. Amongst SRs though there is a large spread, with discy SRs being the most common morphology. Assuming that galaxies evolve from fast rotation to slow via mergers, we would expect to see very few boxy FRs, as boxy shapes could only occur through disrupting a discy ellipsoid. Some merger geometries may still lead to irregular or even discy SRs, and thus the wide variety of SR morphologies are not necessarily a cause for concern. That said, specific choices of the Illustris sub-grid physics, especially the very energetic AGN feedback in the radio mode, leading to fewer wet mergers at lower redshift, probably also play a part in this skew towards discy SRs.

3.5.3 X-ray luminosity

SRs are often observed to have much brighter X-ray emission with respect to the FRs due to significant amounts of gas at $\sim 10^7$ K or above (Pellegrini 2005; Ellis & O’Sullivan 2006). Maintaining gas at these high temperatures may require a large energy input to the gas, which could be delivered by AGN feedback, also explaining the shut-off of star formation. Infalling gas from mergers can also be a source of heating through shocks, though this is likely a secondary effect (Dekel & Birnboim 2006).

We adopt a simple estimate of the X-ray luminosity, L_X , from a bremsstrahlung approximation

$$L_X = 1.2 \times 10^{-24} \frac{1}{m_p^2} \sum_{i=1}^{N_{\text{gas}}} m_{g,i} \rho_{g,i} \mu_i^{-2} T_{g,i}^{\frac{1}{2}} \text{ (erg s}^{-1}\text{)}, \quad (8)$$

where m_p is the mass of a proton, $m_{g,i}$ is the mass of the i th gas cell, $\rho_{g,i}$ and $T_{g,i}$ are gas density and temperature, respectively, and μ_i is the mean molecular weight. We include all gas cells within a radius whose mean density is 200 times the critical density of the Universe and exclude dense, star-forming regions sitting on the effective equation of state (Springel & Hernquist 2003) that would unphysically skew the galaxy to higher luminosities.

The distribution of X-ray luminosities as a function of spin is shown in the bottom panel of Fig. 7. As before, lower mass ($M_* < 10^{11.5} M_\odot$) galaxies (plotted here as pixels) show no clear trends, and most have similar luminosities of $L_X \approx 10^{40} \text{ erg s}^{-1}$

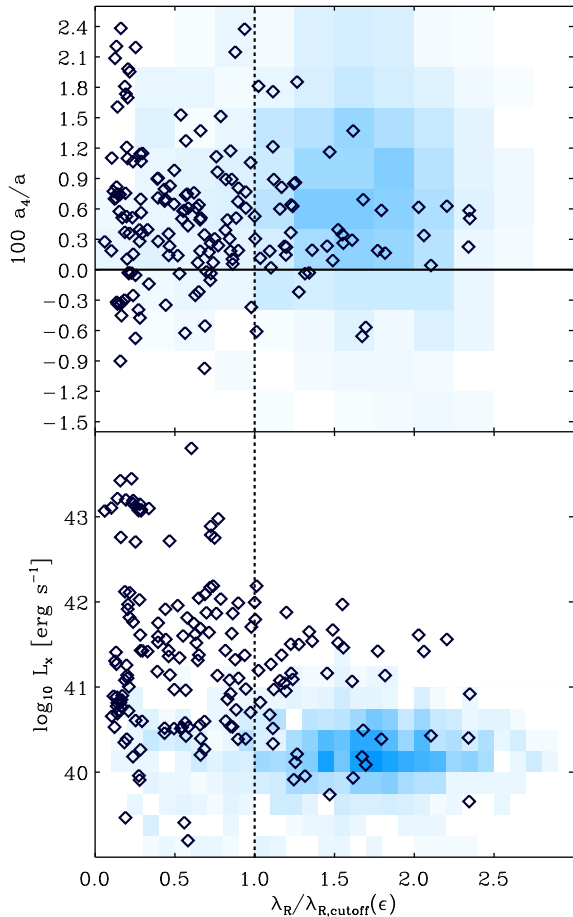


Figure 7. Correlation of λ_R with shape and X-ray luminosity of central elliptical galaxies at $z = 0$. Diamond symbols are for individual galaxies with $M_* > 10^{11.5} M_\odot$, while 2D histograms show galaxies with $M_* < 10^{11.5} M_\odot$. Horizontal axis shows spin normalized by the corresponding cutoff value for each galaxy’s ellipticity ϵ , such that those below a value of 1 are SRs and above are FRs. The vertical axis on the top panel shows the a_4 parameter normalized by the semi-major axis, a , of the fitted ellipse. Solid horizontal line shows the division between discy ellipticals (above) and boxy ellipticals (below). The bottom panel shows the X-ray luminosity, calculated via equation (8).

regardless of spin, though it should be noted that there are few SRs in this sample. Higher mass galaxies (plotted individually as symbols) are generally more luminous, especially some SRs that are two to three orders of magnitude brighter. There is again much variation and only a slight trend for slower spinning high-mass galaxies to be X-ray bright. Note a clear divide between the bulk of galaxies and galaxies with $L_X > 10^{42} \text{ erg s}^{-1}$. We suggest that these particularly bright galaxies are undergoing energetic AGN feedback, heating the gas much more effectively.

There are a variety of other characteristics distinguishing fast and slow rotators, such as the steepness of the Sérsic index, the level of anisotropy/triaxiality and the presence of a strong radio source that we will not examine in this work, while the separation between FRs and SRs in terms of stellar ages and hence metallicities is discussed in the next section.

3.6 Properties of elliptical galaxies

Here we discuss the distribution of various galaxy properties with relevance to their degree of spin and ellipticity, as shown in Fig. 8.

(i) *Stellar mass (top left)*: as previously stated, there is a very strong correlation between a galaxy’s spin and its stellar mass, and we see here that SRs (below the green line) are significantly more massive. We also see a gradient with mass in the FR population (particularly above the magenta line), with rounder, slower spinning FRs being slightly less massive.

(ii) *Gas fraction (top right)*: the fastest rotating galaxies are by far the most gas rich, and the fraction of gas decreases with spin-down to SRs that are almost devoid of gas. There is also a trend among FRs of decreasing gas fraction for rounder slower spinning galaxies.

(iii) *Specific SFRs (middle left)*: SRs are forming almost no stars whilst the fastest spinning FRs are still undergoing significant star formation. Rounder, slower spinning FRs are forming stars at a lower rate than more elongated FRs in agreement with their lower gas fraction.

(iv) *Stellar metallicity (middle right)*: the fastest rotating galaxies are the least enriched, while SRs have highly enriched stars. These results are mirrored in gas metallicity (not shown).

(v) *Stellar half-mass radius (bottom left)*: the distribution of galaxy sizes is very similar in form to the stellar masses [as shown in panel (i)]. The fastest spinning FRs are larger than rounder, slower spinning FRs, and very massive SRs are by far the largest galaxies in the sample.

(vi) *Colour (bottom right)*: SRs are the reddest galaxies in the sample, followed by round FRs and finally elongated FRs, in agreement with gas fraction and metallicity distributions.

In all of these panels, we see strong gradients tracing from the centre of the FR distribution at $(\epsilon, \lambda_R) \approx (0.5, 0.5)$ to the slowest spinning galaxies in the sample at $\sim(0.5, 0.0)$. In many, we also see a gradient along the distribution of FRs, spanning from bottom left to top right of the plots.

Almost all gradients of the former kind can be explained by the gradient in mass. More massive galaxies are likely to undergo more mergers and more AGN feedback, leading to gas being expelled. Gas-poor galaxies then cannot sustain star formation, thus have less short-lived high-mass blue stars and will be redder in colour. The galaxy metallicity is closely related to the age of a galaxy, showing that more massive galaxies must have formed earlier and undergone more bursts of star formation in their lifetimes, possibly fuelled by starburst events during galaxy mergers.

The gradients of the latter kind, across the distribution of FRs, may be driven by efficient galactic wind feedback or by environmental differences. More efficient feedback would expel gas, cutting off star formation and stunting the growth of stellar mass. Alternatively, galaxies in a less gas-rich environment, with only a small supply of inflowing gas, would have less star formation and thus be less massive and smaller. Both mechanisms could explain the transition from spheroid to disc-like morphologies if we assume that the angular momentum of a galaxy comes from that of its inflowing material. Cutting off the supply of gas, either due to a gas-poor environment or by feedback preventing inflowing material reaching the galaxy, could lead to rounder, slower spinning objects.

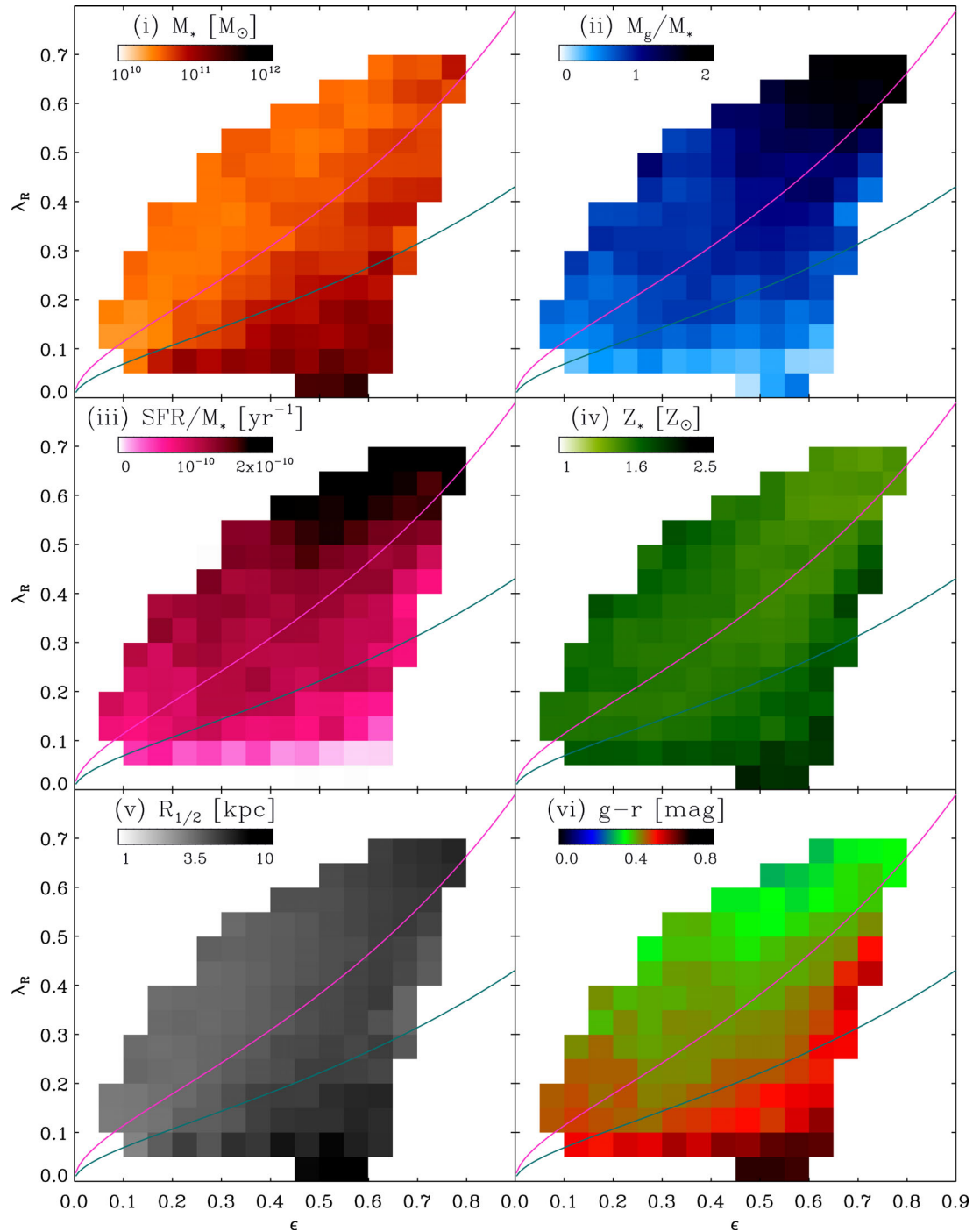


Figure 8. Distribution of various properties of galaxies in the (λ_R, ϵ) space. Top panels show stellar mass (left) and gas mass normalized to the stellar mass (right). Middle panels show specific SFR (left) and stellar metallicity (right). Bottom panels show stellar half-mass radius (left) and $g-r$ colours (right). Results are averaged over snapshots ranging from $z = 0.2$ to 0 and any pixel that does not contain at least 30 galaxies over this period is excluded. Note that SRs are characterized by several distinct properties: large stellar masses, sizes and metallicities, low gas content and specific SFRs, and red colours.

4 MERGER HISTORIES OF FAST AND SLOW ROTATORS

4.1 How progenitor galaxy morphology relates to present-day properties

We begin by separating our sample of 3207 elliptical galaxies at $z = 0$ into FRs and SRs based on our cutoff criteria (see Fig. 4). We

then separate these populations further into high-, intermediate- and low-mass brackets. We follow the main progenitor of each of these galaxies back in time and compare how the distribution of galaxies overall, and the fraction of spiral and elliptical galaxies, varies with mass and kinematic properties.

Examining the main progenitors at $z = 1$, as a function of stellar mass (left-hand panel) and λ_R parameter (right-hand panel) at $z = 0$, as shown in Fig. 9, we see that overall there is very little

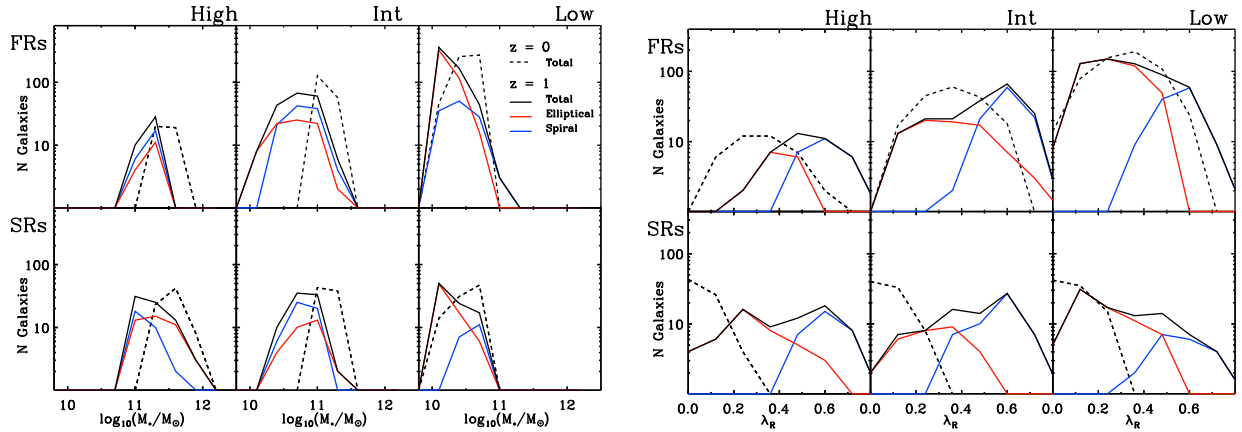


Figure 9. Distribution of main progenitor galaxies at $z = 1$, separated by their properties at $z = 0$ (FRs, SRs and low-, intermediate- and high-mass brackets) in terms of the galaxy’s stellar mass (left-hand panel) and λ_R parameter (right-hand panel) at $z = 0$. The population of galaxies is separated into spirals and ellipticals at $z = 1$. Only galaxies that are well resolvable (over 20 000 star particles) at $z = 1$, and which are classified as ellipticals at $z = 0$, are included.

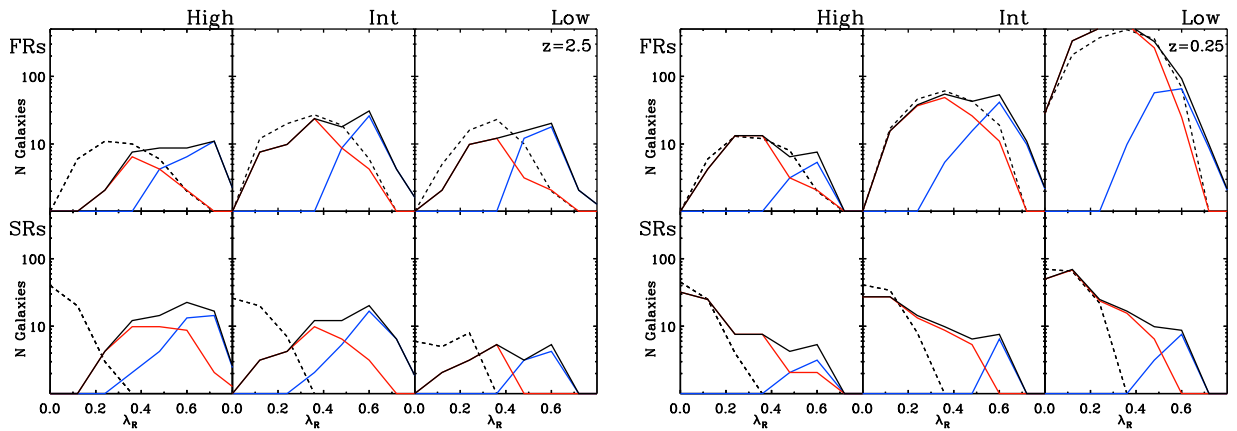


Figure 10. As in Fig. 9, we show the distribution of main progenitor galaxies in terms of their λ_R parameter. Progenitors are shown at $z = 2.5$ (left-hand panel) and $z = 0.25$ (right-hand panel). While at $z = 2.5$ progenitor distributions are very similar, at $z = 0.25$ progenitors of present-day FRs and SRs have clearly different distributions.

difference between the population of galaxies that will eventually diverge to become fast or slow rotators. The highest mass galaxies show the greatest differences, with slightly more high-mass and slow-spinning ellipticals among the progenitors of SRs, but overall the total distribution as well as the fractions and distributions of spirals and ellipticals agree well between FRs and SRs.

This points to the conclusion that the rotational properties of elliptical galaxies are mostly determined by the later half of their evolution. The lack of strong trends in their progenitors suggests that it is the merger histories of the galaxies that are crucial in determining their $z = 0$ kinematics, as this is the major, stochastic, differentiating factor between the later evolution of any two galaxies with similar properties at $z = 1$. In the later sections, we will thus limit our analysis mostly to evolution since $z = 1$.

In Fig. 10, we show the distribution of progenitors at $z = 2.5$ (left-hand panel) and $z = 0.25$ (right-hand panel) with respect to their λ_R parameter. In accord with our previous discussion, at $z = 2.5$ there is almost no difference between FR and SR populations. Despite this redshift being the epoch in which mergers are most prevalent, the lack of any divide between the two populations suggests that either the FR and SR properties are only strongly dependent on recent mergers or that the conditions in which galaxies are evolving,

and mergers are occurring, change significantly after this period. At $z = 0.25$, there is now a clear difference between SR and FR progenitors, with FRs in general being faster spinning and having a higher fraction of spirals. High-mass galaxies have almost converged upon their $z = 0$ distribution, but the same is not true for low- and intermediate-mass galaxies. If rotational properties truly are determined by some mass cutoff, it makes sense that the highest mass galaxies, which have crossed this threshold earlier in time, converge sooner.

An interesting side note in these plots is the re-occurring peak in the distribution of spiral galaxies at $\lambda_R \approx 0.6$ suggesting that spiral galaxies have relatively uniform rotational properties over all redshifts and mass ranges considered. Note further that, as we discussed previously, the resolution and feedback modelling limitations lead to an overestimation of the fraction of elliptical galaxies at low mass (for further details, see Appendix A).

4.2 Examining mechanisms of stellar mass change since $z = 1$

We first examine the relative fraction of stellar mass accreted through major and minor mergers, and the fraction formed *in situ*. We follow the accretion histories of galaxies from $z = 1$ for populations separated by their mass at $z = 0$ (Fig. 11) and

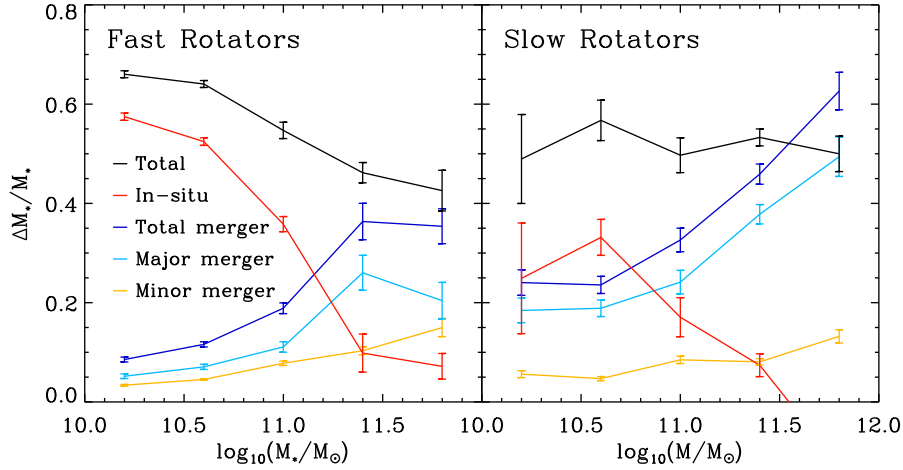


Figure 11. Fraction of mass at $z = 0$ accrued by each elliptical galaxy since $z = 1$, as a function of total mass at $z = 0$, separated into FRs (left) and SRs (right). Different curves, as denoted on the legend, show mass fractions from minor, major and all mergers, *in situ* star formation, as well as the total mass fractions. Points show mean values for all galaxies in each bin, and error bars show error in the mean.

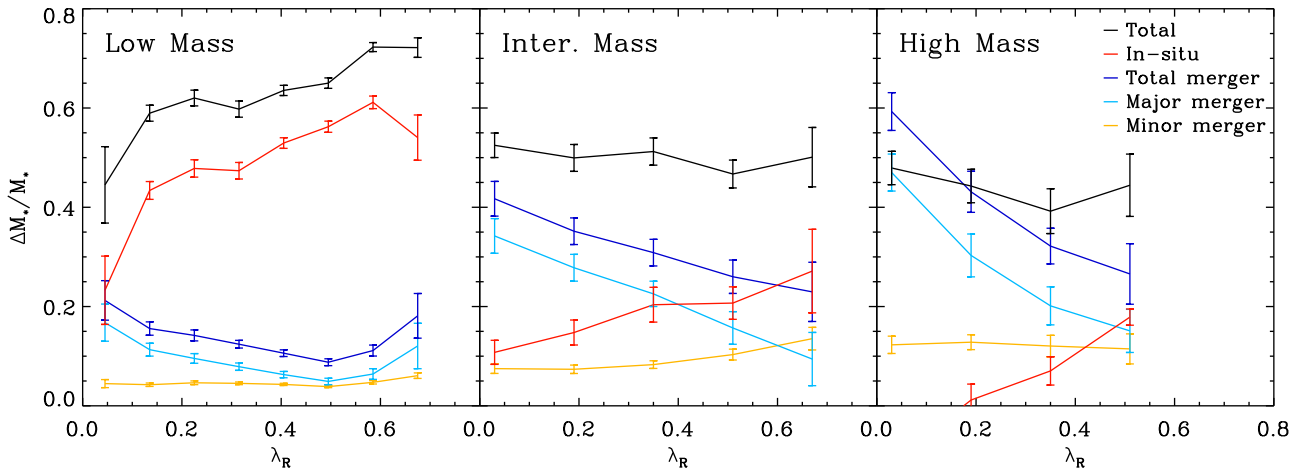


Figure 12. Similar plot to Fig. 11 with galaxies now separated into low- ($M_* < 10^{11} M_\odot$), intermediate- ($10^{11} M_\odot < M_* < 10^{11.5} M_\odot$) and high-mass ($M_* > 10^{11.5} M_\odot$) brackets and plotted as a function of their λ_R values at $z = 0$. Note that the range of values of $\Delta M/M$ is higher for low-mass galaxies and that there are not sufficient numbers of high-mass galaxies at $\lambda_R > 0.5$ for it to be useful to plot these.

rotational properties (Fig. 12). As we have shown in Section 4.1, the kinematic properties of galaxies at $z = 0$ are mostly determined by their evolution in the period post $z = 1$, so by analysing the processes by which they acquire stellar mass in this period, we aim to explain their present-day fast- and slow-rotating properties.

In Fig. 11, we look at how FRs and SRs of different masses accrue their stellar mass in the period since $z = 1$. In both panels, we see some similar trends, i.e. more massive galaxies experience more mergers and gain more mass that way, whilst the amount of mass formed *in situ* decreases. We also see some strong contrasts between FRs and SRs, namely that SRs gain much more of their mass through major mergers and much less through *in situ* star formation, though the total fraction of their mass acquired is similar for both FRs and SRs, as they roughly double their mass in the second half of cosmic time.

We can perform a similar analysis for the three different mass brackets detailed in Section 3.3, this time looking at how accreted mass fraction varies with respect to λ_R values at $z = 0$, as shown in Fig. 12.

For low-mass galaxies, all except the slowest spinning have their mass change dominated by *in situ* star formation. Those with more major mergers seem to be more disrupted. However, by examining the merger histories, there are some low-mass galaxies that have little ordered rotation which have not undergone recent major mergers. This suggests that the process of accreting gas and forming stars, or lack thereof, may alone be able to alter the spin of these galaxies. Minor mergers seem to have very little effect, with more minor mergers possibly very slightly spinning up intermediate-mass galaxies. Intermediate- and high-mass galaxies with a significant mass contribution from major mergers seem to be spun down, whilst *in situ* star formation is associated with a spin-up. We can summarize these results as a simple set of trends.

(i) Slower rotating galaxies have markedly more major mergers in their accretion history; thus, major mergers are linked to a net spin-down.

(ii) Stellar mass change from minor mergers seems to be almost independent of galaxy spin; thus, minor mergers do not significantly affect the spin.

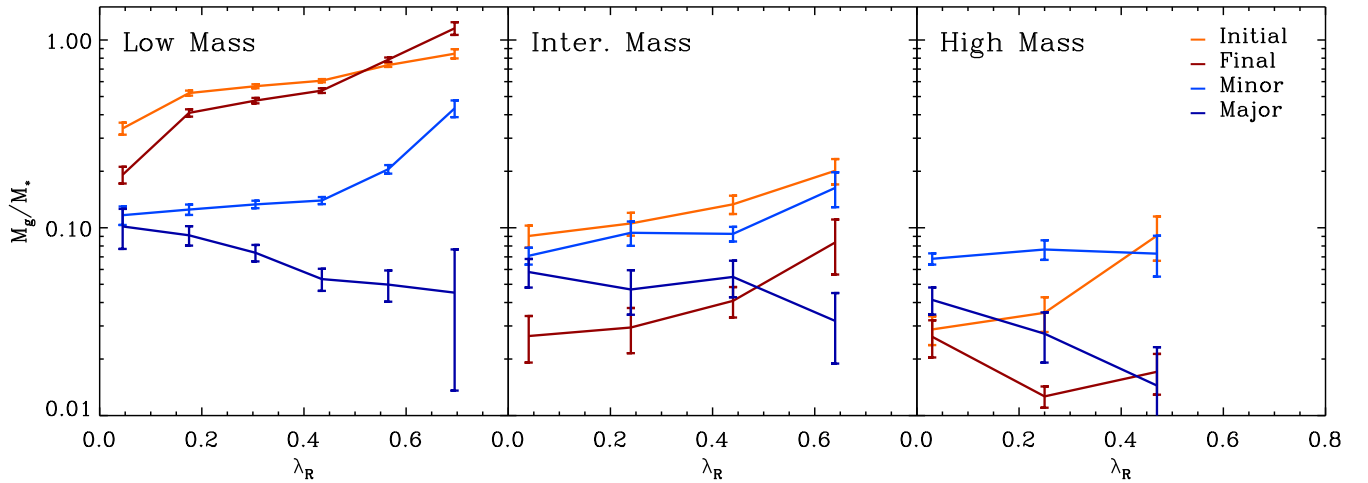


Figure 13. The fraction of gas mass to stellar mass (within two half-mass radii), showing relative amounts at $z = 1$ and 0 along with the accreted gas mass through major and minor mergers during that period. Galaxies are separated into three brackets by their stellar mass and binned by their rotation properties (λ_R) at $z = 0$. All gas masses are shown relative to the stellar mass at $z = 0$.

(iii) Faster rotating galaxies have more *in situ* star formation; thus, star formation is linked to a net spin-up.

The only exception to these trends is the fastest rotating low-mass galaxies, which seem to be spun up by major mergers as well. In fact, the low-mass galaxies with the least mergers have λ_R values closest to the locus of points around which low-mass FRs seem to cluster (Fig. 5). This suggests a scenario in which undisturbed galaxies tend to sit at $\lambda_R \approx 0.5$ unless disturbed by mergers, which in general disrupt spin, but have some small chance of leading to a spin-up and a very fast rotating elliptical galaxy.

These trends however do not give us a clear reason why we should see two distinct populations of FRs and SRs, rather than a continuum. To further examine this, we have to look in more detail at how mergers and *in situ* star formation act on galaxies of different masses.

4.3 Accretion of gas since $z = 1$

Though we trace kinematic properties of galaxies based on their stellar component, gas also plays a large part in the evolution of a galaxy's spin. Inflowing gas may carry a large amount of angular momentum from the intragalactic medium (IGM) to galaxies, and the transfer of energy and angular momentum between stars and gas can be very important.

Fig. 13 shows gas fraction accreted on to galaxies (separated into the same mass brackets) through minor and major mergers, as well as the fraction of gas at $z = 1$ and 0 , as a function of λ_R values at $z = 0$. All gas fractions are calculated with respect to the stellar mass at $z = 0$.

Low-mass galaxies roughly retain their gas content, while the fastest spinning low-mass galaxies even slightly gain gas since $z = 1$. However, as we move towards higher masses, the fraction of gas drastically reduces, due to feedback processes, particularly AGN feedback in the most massive galaxies, which blows almost all the gas out from the centre of the galaxy. Note that for all mass ranges the higher the initial gas fraction, the higher the final λ_R .

In contrast to the previous section, there is now a clear correlation between minor mergers and spin for low- and intermediate-mass galaxies. Perhaps gas-rich minor mergers are a mechanism for replenishing a galaxy's gas supply, or a sign of a gas-rich local

environment. Gas from major mergers does not seem to have the same effect, with slower spinning galaxies gaining more mass from major mergers. We suggest that this is because the major merger is much more damaging to a galaxy, lowering its spin, than any spin-up that might be caused by the injection of gas.

This suggests that the gas component of smaller galaxies is much more effective at transferring angular momentum to the main galaxy than the stellar component, and that the incoming angular momentum is well aligned with the spin of the galaxies, leading to gas-rich minor mergers having a strong spin-up effect. Gas from minor mergers may be a key factor in the evolution of the fastest spinning ellipticals.

There may be a link between the supply of gas, from accretion and minor mergers, and the local environment. Large amounts of gas may be a sign of a high inflow rate from the IGM, and its ability to cool and accrete faster than it is heated and expelled by feedback processes. Incoming gas can spin up a galaxy either by torquing the stellar component or simply by forming new stars with similarly high angular momentum.

Putting together this evidence, we conclude the following.

- (i) The supply of gas to a galaxy is closely linked to its spin, with more gas leading to faster spinning, more ordered rotation.
- (ii) Gas-rich minor mergers are linked to a spin-up in lower mass galaxies.
- (iii) Major mergers, regardless of gas content, are linked to a spinning down of galaxies.

4.4 Evolution of galaxies during mergers

We can roughly separate the history of a galaxy's evolution into long periods without any major merger activity and the short periods over which a major merger is rapidly changing the galaxy.

As shown in the previous section, the rotation properties of massive ellipticals have a strong correlation with the fraction of stellar and gas mass accreted through major mergers. Thus, we examine in Fig. 14 the change in λ_R following a major merger as a function of time. Solid curves are for times directly after the major merger (from two to eight snapshots afterwards, roughly corresponding to 0.25 and 1 Gyr, respectively), while dashed curves show the result

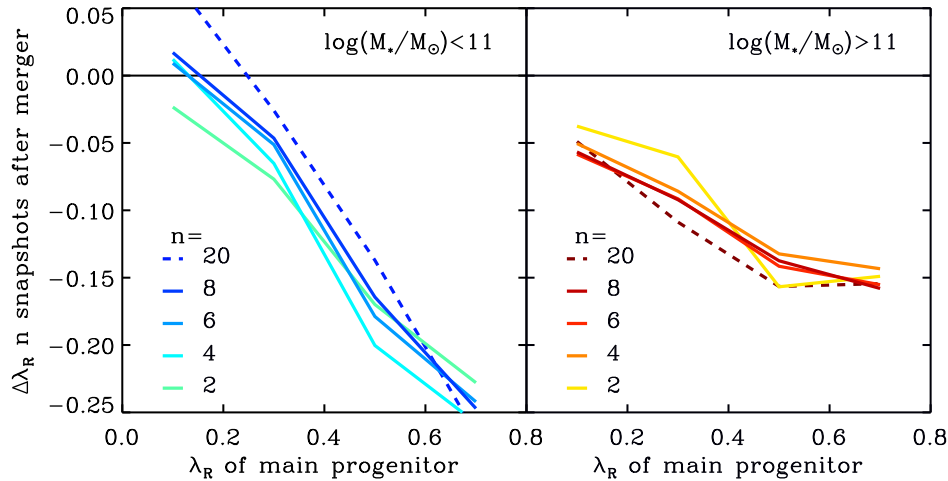


Figure 14. Change in λ_R for major mergers occurring since $z = 1$, plotted against the initial λ_R of the more massive progenitor galaxy. The resulting change, relative to initial λ_R , is shown 2, 4, 6, 8 and 20 snapshots after the merger itself, and results are separated for low-mass galaxies (left) and high-mass galaxies (right). For reference, snapshots are spaced in time intervals of roughly 0.1–0.15 Gyr.

after a longer period of time (20 snapshots, roughly corresponding to 2.5 Gyr).

For galaxies of all masses, a major merger causes an immediate and drastic disruption of any ordered rotation. It should be noted that this is an average effect, and some small fraction of major mergers can still lead to a spin-up of the remnant. For all but the slowest rotating galaxies, for which the value of λ_R cannot drop any further, low-mass ellipticals are more immediately disrupted by major mergers than higher mass galaxies, losing almost half their spin in a single major merger.

For lower mass galaxies, it takes around 0.5 Gyr (two to four snapshots) for the value of λ_R to reach a minimum, after which their spin gradually begins to increase again, showing signs of recovering from the effect of the merger. No such recovery of spin post-merger is seen in high-mass galaxies. Shortly after the merger, they seem to settle in a slower spinning configuration. Though each individual merger has less disruptive effect on higher mass galaxies, the fact that they do not seem to recover their spin post-merger suggests that repeated major mergers can reduce the galaxy’s spin in steps.

We then investigated further the factors leading to a galaxy spinning up again after a merger. As shown in Fig. 15, we found a strong dependence on the gas fraction shortly after the merger, with galaxies that retained gas quickly recovering spin. This seems to be the case for all mass ranges, though as there is a strong dependence on gas fraction with galaxy mass, it would explain why we see little spin-up of merger remnants in high-mass galaxies. It could also explain the dependence of spin properties on gas fraction (Fig. 13) as only galaxies with sufficient gas mass would recover their spin post-merger.

From this, we can draw some general trends of how galaxies are affected by major mergers.

- (i) On average, major mergers strongly disrupt the spin of elliptical galaxies.
- (ii) Galaxies that are more gas rich post-merger recover a significantly higher degree of spin.
- (iii) Thus, low-mass galaxies, which are in general gas rich, begin to recover their spin post-merger whilst high-mass galaxies, which are much more gas poor, do not.

We looked at the relative effect of wet and dry mergers (those for which the incoming galaxies are gas rich or gas poor) and saw

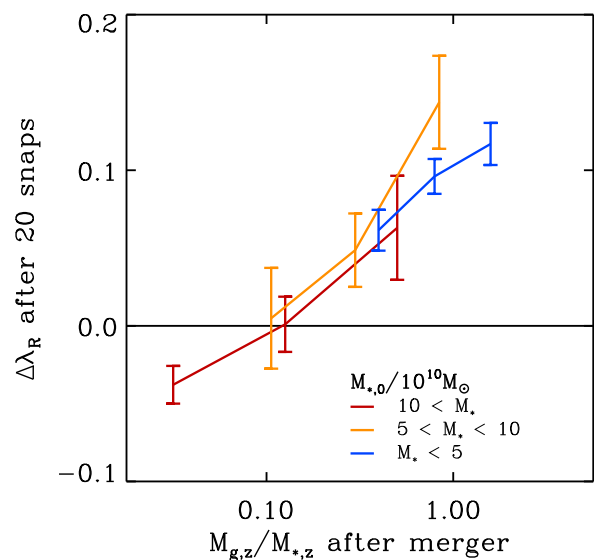


Figure 15. Change in λ_R 2–3 Gyr (20 snapshots) after a major merger occurring since $z = 1$, plotted against the fraction of gas mass to stellar mass (within two half-mass radii) directly following the merger (after ~ 0.33 Gyr or three snapshots).

very little qualitative difference. Rodriguez-Gomez et al. (2017) performed similar analysis on Illustris galaxies, specifically investigating galaxies with κ above and below 0.5 (corresponding by our definitions to spirals and ellipticals, respectively), and found no discernible correlation between wet/dry mergers and galaxy morphology for all but the most massive galaxies. Lagos et al. (2017) also look at the effects of wet and dry mergers in the EAGLE simulation, finding wet (dry) mergers leading to a spin up (down), though they categorise mergers based on total gas content of the system, not just of the incoming galaxy. There seems to be much more dependence on the gas content of the main progenitor and the merger remnant, than that of the incoming galaxy.

4.5 Evolution of galaxies without major mergers

For most galaxies, especially in the later half of their evolution, major mergers are rare events and most of their lifetime is dominated

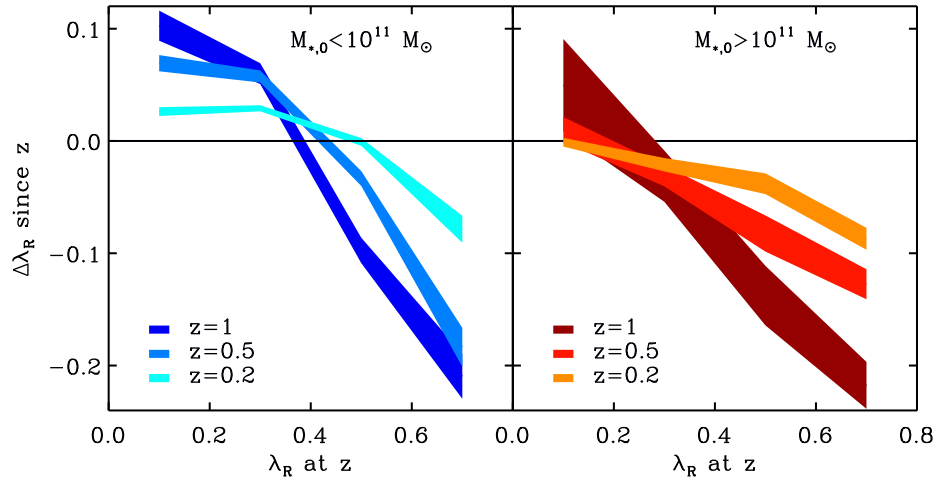


Figure 16. Change in λ_R for galaxies with negligible mass accretion from major mergers (<1 percent of ΔM_*) as a function of $\lambda_R(z)$ over a period from a given redshift, z (see the legend) to $z = 0$.

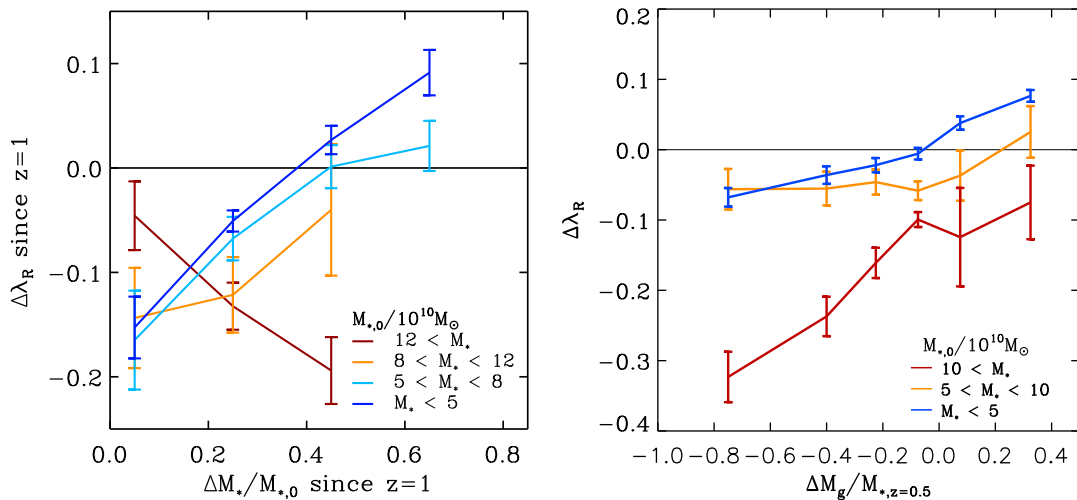


Figure 17. Left: change in λ_R for galaxies as a function of their increase in stellar mass since $z = 1$, for galaxies with negligible major mergers. Right: change in λ_R since $z = 0.5$ as a function of a galaxy’s gas inflow and outflow in that period. Shown only for galaxies with no major mergers in this period. Change in gas mass includes gas used in star formation as well as galactic inflow and outflow, and is normalized by the stellar mass at $z = 0.5$.

by long periods of slow evolution. As minor mergers have small effects individually, and are frequent enough to be seen as roughly steady accretion of matter, they will be treated as part of this gradual evolution. We have shown that a galaxy’s spin is strongly correlated with the amount of gas associated with a galaxy, and with the amount of stellar mass formed through *in situ* star formation. Thus, we want to ask the question of what happens to a galaxy that is left to its own devices, forming stars and growing steadily in the absence of major mergers.

Fig. 16 shows how λ_R changes over the period leading up to $z = 0$ for galaxies with little or no mass accreted through major mergers, split between low- and high-mass galaxies. Roughly half of the total sample of galaxies have no major mergers since $z = 0.5$, with the fraction being slightly smaller at higher masses. Excluding also those galaxies with any significant mass gain via minor mergers does not change the trends seen, but leads to increased noise.

We see that fast-spinning low-mass galaxies are spun down and slow-spinning galaxies are spun up. This suggests that low-mass galaxies with no major external influences will equilibrate to some intermediate value of λ_R . As time goes on, this equilibrium value

seems to increase, and close to $z = 0$ it is roughly $\lambda_R = 0.5$, which coincides well with the locus of points around which low-mass galaxies are clustered in Fig. 5.

In contrast, high-mass galaxies that are initially spinning slowly are not spun up. Even those galaxies with the lowest λ_R show no significant increase in their spin after $z = 1$; thus, there is no similar equilibrium spin (or looked at from another perspective, the equilibrium spin value is $\lambda_R \rightarrow 0$). Fast-spinning massive galaxies are still naturally spun down over time.

This behaviour could be key to the two separate populations of FRs and SRs. If more massive galaxies tend not to be spun up even when they are spinning slowly, infrequent major mergers would still be effective at reducing their spin by a large amount over time. In contrast, lower mass galaxies, even if they undergo a cataclysmic event, could then recover that spin in the long periods between major mergers.

The left-hand panel of Fig. 17 shows how the spin properties change, for galaxies in different mass bins, depending on the change in their stellar mass. As galaxies with major mergers are excluded, the main avenue for these galaxies to gain mass is through minor

mergers and *in situ* star formation (as before excluding galaxies with significant mass change through minor mergers gives behaviour that is qualitatively the same, but with much more noise in the data).

For low and intermediate masses, we see that there is a tendency for galaxies with little or no stellar mass gain to spin down. For high-mass galaxies, this seems to be less effective, possibly because they are already slow spinning at $z = 1$ and hence there is a minimum possible drop in λ_R . For lower mass galaxies, the more mass gained, the more the galaxy is spun up. This is because the stellar mass gain is associated mostly with *in situ* star formation from accreting gas, which has a significant angular momentum.

As we move to higher mass bins, the spin-up process seems to be less effective, and for the most massive galaxies the trend is reversed: the more stellar mass gained, the more the spin is disrupted. One could interpret this by saying that above a critical mass we transition to stellar mass growth being more associated with minor mergers than *in situ* star formation, though this would be in contrast with the absence of any dependence on minor mergers in Figs 11 and 12, unless many very small merging galaxies are unnoticed by the halo finder. Instead, more likely it could be due to a change in the geometry of accretion, with incoming gas no longer adding angular momentum coherent with the galaxies' spin, either due to change in the local environment due to the galaxy itself (such as through heating via AGN) or due to the galaxy's location, as higher mass galaxies tend to sit in galaxy groups and clusters.

Finally, we compare the change in spin due to gas accretion and expulsion (excluding mergers). Without following the flow of gas in individual cells, this is an inexact art, but we can estimate the mass of gas inflowing and outflowing, ΔM_g , using $\Delta M_g = M_{g,z} - M_{g,0} - \Sigma \Delta M_{g,\text{mergers}} + \Delta M_{*,\text{situ}}$. This assumes that the vast majority of gas that forms stars is external to a galaxy. Obviously, this can be negative when outflow driven by feedback blows more mass outwards in this period than the galaxy is able to accrete.

The right-hand panel of Fig. 17 shows the change in spin of galaxies as a function of their ability to accrete or blow out gas between $z = 0.5$ and 0. Only amongst low-mass galaxies, inflow can dominate over outflow, and for those the inflowing gas is linked to a spin-up. High-mass galaxies tend to expel significantly more gas than they accrete, and whilst they show similar trends, they lose much more spin in the same time period compared to their lower mass counterparts.

For all galaxies, high level of feedback and gas expulsion lead to a spin-down as the outflowing gas takes with it angular momentum, and tends to redistribute the angular momentum (hence disrupt the ordered rotation) of star particles. Though net gas inflow/outflow may be small, galaxies may still experience strong feedback and rapid accretion, roughly cancelling each other out. Thus, it is possible that high-mass galaxies are more disrupted because they are all experiencing large amounts of feedback but replenishing some mass via accretion.

We suggest this shift in behaviour for galaxies above $\sim 10^{11} M_\odot$ to be either due to environment or feedback. These massive galaxies are less likely to be found in cosmic filaments and more likely in clusters, leading to a different, more isotropic, geometry of accretion. Equally, at around this mass, the dominant mode of feedback shifts from that associated with star formation to AGN, which is a much more violent feedback mechanism. The shift could also be due to the rising level of minor mergers, but the lack of dependence shown earlier dissuades this idea.

Thus, for a typical galaxy left to evolve gradually under accretion of gas, we see the following trends.

- (i) Fast-spinning galaxies, of all masses, naturally spin down over time.
- (ii) Low-mass slow-spinning galaxies spin up over time, leading them to equilibrate. High-mass galaxies do not show such recovery and hence never regain their spin.
- (iii) Gas accretion and associated star formation are linked to a spin-up of a galaxy, but in high-mass galaxies, mass growth leads to a spin-down.

The qualitative results remain unchanged when examining separately those galaxies with the negligible mass gain through minor mergers, and those for which minor mergers are dominant.

5 CONCLUSIONS AND DISCUSSION

Using the cosmological hydrodynamic simulation Illustris, we have followed thousands of massive elliptical galaxies back across cosmic time to understand and explain how their rotation properties developed. Separating present-day ellipticals into fast and slow rotators (FRs and SRs), we sought to explain how some massive galaxies maintain ordered motion and disc-like rotation, whilst others lose order in their stellar orbits, developing complex velocity fields dominated by dispersion.

5.1 Present-day properties of fast and slow rotators

We first construct a small subset of Illustris galaxies to match the observed ATLAS^{3D} sample of elliptical galaxies (E+11), finding very similar fraction of SRs (~ 14 percent), which are all mostly massive galaxies, while FRs are predominantly low-mass galaxies ($M_* < 10^{11} M_\odot$), as found in observations as well. If we extend our analysis to all well-resolved elliptical galaxies in Illustris (with at least 20 000 star particles, or $M_* \gtrsim 10^{10.5} M_\odot$), the fraction of SRs stays similar, indicating that we have a representative sample of SRs and FRs. While qualitative agreement with the ATLAS^{3D} survey is very encouraging, we find a discrepancy in the ellipticities of SRs, which appear more elongated in Illustris than in the observed sample. Similar behaviour was seen in previous work, such as N+14 and Bois et al. (2010), which concluded that too gas-poor mergers can lead to galaxies with artificially high ellipticities.

By separating galaxies into three mass bins, we see two clear loci around which galaxies cluster. Low-mass galaxies are a smoothly distributed population of FRs (centred on the same point as spiral galaxies would be, though with more dispersion). High-mass galaxies are mostly, but not all, part of a wholly separate distribution of SRs. Intermediate-mass galaxies ($10^{11} M_\odot < M_* < 10^{11.5} M_\odot$) can fall at either locus or be smoothly distributed between them.

Looking back to earlier redshifts, the distribution of ellipticals is largely unaltered: there are fewer and fewer high-mass galaxies and correspondingly fewer SRs, but low- and intermediate-mass galaxies tend to lie in a similar distribution to the one at $z = 0$, possibly with a slight shift to higher ellipticities. The population of host galaxies and satellites also appears to be congruent, again with the exception that there are very few high-mass satellites and hence the vast majority of SRs are host galaxies.

Whilst we mostly focus on a kinematic classification of fast and slow rotators, we also examine various other characteristics that separate the two populations. We test for central cores and cusps, boxy and discy isodensity contours, and X-ray emission from hot gas. High-mass ellipticals obey known observational relationships well, particularly their X-ray luminosity, whilst lower mass galaxies limited by resolution have much less clear trends.

We further examine how other galaxy properties, such as stellar mass, gas fraction, metallicity and colour, relate to kinematic properties. The fraction of gas, compared to stellar mass, decreases almost uniformly with decreasing spin, with SFR and colour closely coupled to this trend. Stellar mass increases sharply as we transition from fast to slow rotators, and there is also a possible gradient from low-mass spheroidal FRs to higher mass elongated FRs. The mass gradient is mirrored in the stellar half-mass radii of these galaxies. SRs also have higher metallicity, both in stars and gas. Fast-spinning spheroidal FRs are also particularly enriched, and we suggest that this may be due to starbursts during mergers that could have also spun them up.

5.2 Redshift evolution of fast and slow rotators

To understand how evolutionary history impacts on the present-day kinematical properties of galaxies, we have followed the first progenitor of $z = 0$ galaxies back in time, finding that there is little difference at $z = 1$ between galaxies that will become FRs and SRs and no discernible difference at higher redshift. A divergence in the populations is apparent from $z = 0.25$, leading us to conclude that it is evolution in the later part of a galaxy's life, during which the major differentiating factor is their stochastic merger histories, that determines an elliptical galaxy's rotation properties.

We can separate the mechanisms acting on an elliptical galaxy in this late stage of its life and the effect they have as follows.

(a) *Major mergers.* We find that in general, across all mass ranges and regardless of gas fraction, an incoming massive galaxy tends to lead to a huge disruption and a slower spinning merger remnant (see also e.g. Barnes & Hernquist 1996; Cox et al. 2006; Hoffman et al. 2009; Jesseit et al. 2009). That said, rare major mergers, potentially with specific geometries for the collision, can lead to an increase in spin (see also Naab, Khochfar & Burkert 2006b; Di Matteo et al. 2009; Bois et al. 2010, 2011). The fate of a galaxy undergoing such a collision is in large part dependent on factors relating to encounter geometries, which we do not explore in this paper.

Even after the more common highly disruptive mergers, galaxies may recover their spin. Gas-rich galaxies, or those in a gas-rich environment, which still have a significant gas mass directly after a merger, tend to spin back up. This means that galaxies can undergo major mergers and remain fast rotators. Galaxies that do not recover their spin after the merger can, by either a single merger or repeated encounters, become completely disrupted and end up as slow rotators.

(b) *Minor mergers.* In contrast to some previous works (Bournaud, Jog & Combes 2007; Qu et al. 2010), we have found little or no dependence on minor mergers for determining the spin of an elliptical galaxy. Minor mergers account for only a small fraction of the mass growth of a galaxy since $z = 1$, independent of the galaxy's spin. The only strong trend seen is that minor mergers that bring in large amounts of gas to low- and intermediate-mass galaxies are associated with a spin-up and may be the origin of some of the fastest spinning galaxies.

This may, however, depend on the scale of incoming body that we term a minor merger. What we see as part of the steady accretion of material may actually be a bombardment by bound objects so small as to not be identifiable to our halo finders. Thus, some of the results outlined below, for steady accretion of gas and stars, may by another nomenclature be included as an effect of minor mergers.

Early results from the MaNGA survey show no discernable differences between the λ_R, ϵ distribution for central and satellite galaxies (Greene et al., in preparation), and they suggest that this shows that the number of minor mergers (which is strongly dependent on environment) does not have a large impact on spin evolution.

(c) *Accretion of stars and gas.* For low-mass galaxies, accreting gas and forming stars leads to a spin-up, most likely from the incoming angular momentum of accreted material adding coherently to the spin of the galaxy. In higher mass galaxies, this ceases to be the case; the rate of gas inflow is smaller and tends to be less than the feedback-driven outflow, and new stars forming and accreting seem to disrupt the galaxy's spin.

We suggest two plausible mechanisms for this dichotomy. The transition could be environmental, with higher mass galaxies more likely to sit at the centres of gas-poor clusters. Thus, only a small amount of gas is inflowing, and possibly coming in at such an angle that it diminishes the net angular momentum of the galaxy. The transition could also be dependent on the type of feedback, as at these higher masses AGN feedback becomes dominant, and this more violent feedback may disrupt the galaxy further or prevent incoming gas transferring angular momentum to the galaxy effectively. Differentiating between these two situations is beyond the scope of this work but provides an interesting avenue for further study.

5.3 The origin of fast and slow rotators

Putting together all of our results, we can attempt to explain the origin of fast and slow rotators.

Fast rotators. Fast-rotating elliptical galaxies are mostly lower mass galaxies with a plentiful supply of gas that even after major mergers are able to recover their spin and tend to equilibrate to a certain degree of spin ($\lambda_R \approx 0.5$).

High levels of gas inflow can spin them up, and over periods with little accretion they will spin down. Across the population, accretion rates do not vary greatly, and they tend to share similar rotation properties. Major mergers tend to disrupt their spin, though in rare fortuitous cases can lead to faster rotation.

In terms of spin and mass, their properties are close to those of spiral galaxies, which sit tightly distributed around $(\lambda_R, \epsilon) = (0.5, 0.55)$, suggesting that FRs are part of the natural evolution from lower mass spirals and all ellipticals may have spent part of their life as FRs.

Slow rotators. Slow-rotating elliptical galaxies are older and more massive. They seem to have evolved from fast rotators and done so between $z = 1$ and 0. They are generally gas poor, with most of their incoming mass coming from mergers, and tend only to lose spin as they grow, without recovering it.

The key divide between FRs and SRs is that the latter are not spun up by accreting gas and stars. Even in periods without major mergers, the accumulation of new stellar mass causes them to lose spin, and they expel gas more quickly than it can accrete. This shift, in how the galaxy reacts to incoming mass, may be either environmental, with changes in the local temperature, abundance and geometry of accreting gas, or it may be intrinsic, with the shift towards powerful AGN feedback preventing the transfer of angular momentum from accreting material by heating inflowing gas and disrupting or diverting its accretion. Either way, slow rotators tend to atrophy in their old age, at best retaining what spin they have, at worst slowly spinning down.

Whilst SRs can be created without mergers, these more massive galaxies also have the highest frequency of major mergers. This

repeated bombardment lowers their degree of ordered rotation in large steps. Lower mass galaxies that suffer uncommonly frequent or disruptive mergers can also lose spin faster than they recover it, accounting for a small population of lower mass SRs (though, as stated above, these may soon regain their spin and become FRs afresh). Major mergers may infrequently cause a spin-up, leading to high-mass galaxies, which undergo the most mergers, having the highest spread of spin properties. Eventually, however, as an FR grows in mass, it loses most of its spin, whether by degree or in great bounds, and settles as a near-completely-disordered SR.

Finally, we can compare our results with those of *N+14*, who presented the previous most in-depth analysis of FR and SR evolution, and with whom we find in general excellent agreement. They present detailed histories of a small number of galaxies and present six evolutionary pathways (three each) for fast and slow rotators. All six paths fit within our much broader scheme, though some are shown to be much less frequent on a population scale (such as rare major mergers leading to a spin-up). The only major difference between their results and ours is that they found strong dependence on whether mergers were gas rich or poor. We find that this has little effect on a galaxy's spin, but instead that the amount of gas the main progenitor galaxy has and retains before and after the merger has a large effect. Where they present detailed histories of a few specific galaxies, we show how these extend to a general cosmological population.

Currently, large galaxy surveys such as ATLAS^{3D}, CALIFA, MaNGA and SAMI are starting to provide comprehensive galaxy samples with a wealth of spatially resolved, kinematical properties. By carefully comparing large-scale hydrodynamical simulations, such as Illustris, with these unique data sets, as we have done in this paper, we can gain new insights into the intricate process of galaxy formation and assembly, which will allow us to build a more complete theoretical picture of how galaxies grow and evolve.

ACKNOWLEDGEMENTS

We would like to thank Eric Emsellem, Jenny Greene and Vicente Rodriguez-Gomez for their excellent thoughts, comments and questions. BPM acknowledges support from the Kavli Foundation and the German Science Foundation (DFG) for an Emmy Noether grant. The Flatiron Institute is supported by the Simons Foundation. DS acknowledges support by the STFC and the ERC Starting Grant 638707 'Black holes and their host galaxies: co-evolution across cosmic time'.

REFERENCES

Barnes J. E., 1988, *ApJ*, 331, 699
 Barnes J. E., 1998, in Kennicutt R. C., ed., *Saas-Fee Advanced Course 26, Galaxies: Interactions and Induced Star Formation*. Springer-Verlag, Berlin, p. 275
 Barnes J. E., Hernquist L., 1996, *ApJ*, 471, 115
 Behroozi P. S., Conroy C., Wechsler R. H., 2010, *ApJ*, 717, 379
 Bekki K., Shioya Y., 1997, *ApJ*, 478, L17
 Bender R., 1988, *A&A*, 193, L7
 Bender R., Nieto J., 1990, *A&A*, 239, 97
 Bender R., Doebereiner S., Moellenhoff C., 1988, *A&AS*, 74, 385
 Bender R., Surma P., Doebereiner S., Moellenhoff C., Madejsky R., 1989, *A&A*, 217, 35
 Bendo G. J., Barnes J. E., 2000, *MNRAS*, 316, 315
 Binney J., 2005, *MNRAS*, 363, 937
 Bois M. et al., 2010, *MNRAS*, 406, 2405

Bois M. et al., 2011, *MNRAS*, 416, 1654
 Bottrell C., Torrey P., Simard L., Ellison S. L., 2017, *MNRAS*, 467, 1033
 Boselli A. et al., 2014, *A&A*, 570, A69
 Bournaud F., Jog C. J., Combes F., 2007, *A&A*, 476, 1179
 Bridge C. R. et al., 2007, *ApJ*, 659, 931
 Bryan G. L. et al., 2014, *ApJS*, 211, 19
 Cappellari M. et al., 2007, *MNRAS*, 379, 418
 Cappellari M. et al., 2011, *MNRAS*, 413, 813
 Carlberg R. G., 1986, *ApJ*, 310, 593
 Chabrier G., 2003, *PASP*, 115, 763
 Choi H., Yi S. K., 2017, *ApJ*, 837, 68
 Conselice C. J., 2006, *MNRAS*, 373, 1389
 Cox T. J., Dutta S. N., Di Matteo T., Hernquist L., Hopkins P. F., Robertson B., Springel V., 2006, *ApJ*, 650, 791
 Crain R. A. et al., 2015, *MNRAS*, 450, 1937
 Davies R. L., Efstathiou G., Fall S. M., Illingworth G., Schechter P. L., 1983, *ApJ*, 266, 41
 Davis M., Efstathiou G., Frenk C. S., White S. D. M., 1985, *ApJ*, 292, 371
 De Lucia G., Blaizot J., 2007, *MNRAS*, 375, 2
 Dekel A., Birnboim Y., 2006, *MNRAS*, 368, 2
 Di Matteo P., Jog C. J., Lehnert M. D., Combes F., Semelin B., 2009, *A&A*, 501, L9
 Dolag K., Borgani S., Murante G., Springel V., 2009, *MNRAS*, 399, 497
 Dubois Y. et al., 2014, *MNRAS*, 444, 1453
 Ellis S. C., O'Sullivan E., 2006, *MNRAS*, 367, 627
 Ellison S. L., Mendel J. T., Patton D. R., Scudder J. M., 2013, *MNRAS*, 435, 3627
 Emsellem E. et al., 2007, *MNRAS*, 379, 401
 Emsellem E. et al., 2011, *MNRAS*, 414, 888 (E+11)
 Faber S. M. et al., 1997, *AJ*, 114, 1771
 Fall S. M., Efstathiou G., 1980, *MNRAS*, 193, 189
 Genel S. et al., 2014, *MNRAS*, 445, 175
 Gerhard O. E., 1981, *MNRAS*, 197, 179
 Guo Q., White S., Li C., Boylan-Kolchin M., 2010, *MNRAS*, 404, 1111
 Hernquist L., 1993, *ApJ*, 409, 548
 Hinshaw G. et al., 2013, *ApJS*, 208, 19
 Hirschmann M., Dolag K., Saro A., Bachmann L., Borgani S., Burkert A., 2014, *MNRAS*, 442, 2304
 Hoffman L., Cox T. J., Dutta S., Hernquist L., 2009, *ApJ*, 705, 920
 Hopkins P. F., 2015, *MNRAS*, 450, 53
 Hopkins P. F., Hernquist L., Cox T. J., Dutta S. N., Rothberg B., 2008, *ApJ*, 679, 156
 Hu C.-Y., Naab T., Walch S., Moster B. P., Oser L., 2014, *MNRAS*, 443, 1173
 Jesseit R., Naab T., Peletier R. F., Burkert A., 2007, *MNRAS*, 376, 997
 Jesseit R., Cappellari M., Naab T., Emsellem E., Burkert A., 2009, *MNRAS*, 397, 1202
 Joachimi B., Semboloni E., Bett P. E., Hartlap J., Hilbert S., Hoekstra H., Schneider P., Schrabback T., 2013, *MNRAS*, 431, 477
 Khandai N., Di Matteo T., Croft R., Wilkins S., Feng Y., Tucker E., DeGraf C., Liu M.-S., 2015, *MNRAS*, 450, 1349
 Kormendy J., 2016, in Laurikainen E., Peletier R., Gadotti D., eds, *Astrophysics and Space Science Library*, Vol. 418, *Galactic Bulges*. Springer, Berlin, p. 431
 Kormendy J., Bender R., 1996, *ApJ*, 464, L119
 Kormendy J., Bender R., 2012, *ApJS*, 198, 2
 Kormendy J., Fisher D. B., Cornell M. E., Bender R., 2009, *ApJS*, 182, 216
 Krajnovic D. et al., 2011, *MNRAS*, 414, 2923
 Lagos C. del P., Theuns T., Stevens A. R. H., Cortese L., Padilla N. D., Davis T. A., Contreras S., Croton D., 2017, *MNRAS*, 464, 3850
 Lake G., 1989, *AJ*, 97, 1312
 Larson R. B., 1969, *MNRAS*, 145, 405
 Lauer T. R. et al., 1995, *AJ*, 110, 2622
 Merritt D., 2006, *ApJ*, 648, 976
 Mo H., van den Bosch F. C., White S., 2010, *Galaxy Formation and Evolution*. Cambridge Univ. Press. Cambridge
 Moster B. P., Somerville R. S., Maulbetsch C., van den Bosch F. C., Macciò A. V., Naab T., Oser L., 2010, *ApJ*, 710, 903

Moster B. P., Macciò A. V., Somerville R. S., Naab T., Cox T. J., 2011, *MNRAS*, 415, 3750

Moster B. P., Naab T., White S. D. M., 2013, *MNRAS*, 428, 3121

Moster B. P., Macciò A. V., Somerville R. S., 2014, *MNRAS*, 437, 1027

Muzzin A. et al., 2013, *ApJ*, 777, 18

Naab T., Burkert A., 2003, *ApJ*, 597, 893

Naab T., Burkert A., Hernquist L., 1999, *ApJ*, 523, L133

Naab T., Jesseit R., Burkert A., 2006a, *MNRAS*, 372, 839

Naab T., Khochfar S., Burkert A., 2006b, *ApJ*, 636, L81

Naab T., Johansson P. H., Ostriker J. P., Efstathiou G., 2007, *ApJ*, 658, 710

Naab T. et al., 2014, *MNRAS*, 444, 3357 (N+14)

Negroponte J., White S. D. M., 1983, *MNRAS*, 205, 1009

Nelson D. et al., 2015, *Astron. Comput.*, 13, 12

Partridge R. B., Peebles P. J. E., 1967, *ApJ*, 147, 868

Pellegrini S., 2005, *MNRAS*, 364, 169

Qu Y., Di Matteo P., Lehnert M., van Driel W., Jog C. J., 2010, *A&A*, 515, A11

Remus R.-S., Dolag K., Naab T., Burkert A., Hirschmann M., Hoffmann T. L., Johansson P. H., 2017, *MNRAS*, 464, 3742

Robertson B., Bullock J. S., Cox T. J., Di Matteo T., Hernquist L., Springel V., Yoshida N., 2006, *ApJ*, 645, 986

Rodriguez-Gomez V. et al., 2015, *MNRAS*, 449, 49

Rodriguez-Gomez V. et al., 2016, *MNRAS*, 458, 2371

Rodriguez-Gomez V. et al., 2017, *MNRAS*, 467, 3083

Sales L. V., Navarro J. F., Theuns T., Schaye J., White S. D. M., Frenk C. S., Crain R. A., Dalla Vecchia C., 2012, *MNRAS*, 423, 1544 (S+12)

Schaye J. et al., 2015, *MNRAS*, 446, 521

Schweizer F., 1982, *ApJ*, 252, 455

Sijacki D., Vogelsberger M., Kereš D., Springel V., Hernquist L., 2012, *MNRAS*, 424, 2999

Sijacki D., Vogelsberger M., Genel S., Springel V., Torrey P., Snyder G. F., Nelson D., Hernquist L., 2015, *MNRAS*, 452, 575

Snyder G. F. et al., 2015, *MNRAS*, 454, 1886

Springel V., 2010, *MNRAS*, 401, 791

Springel V., Hernquist L., 2003, *MNRAS*, 339, 289

Springel V., Yoshida N., White S. D. M., 2001, *New Astron.*, 6, 79

Tasca L. A. M. et al., 2014, *A&A*, 565, A10

Tenneti A., Mandelbaum R., Di Matteo T., Feng Y., Khandai N., 2014, *MNRAS*, 441, 470

Teysier R., 2002, *A&A*, 385, 337

Toomre A., 1977, in Tinsley B. M., Larson R. B. eds, *Evolution of Galaxies and Stellar Populations*. Yale University Observatory, New Haven, p. 401

Toomre A., Toomre J., 1972, *ApJ*, 178, 623

Vogelsberger M., Genel S., Sijacki D., Torrey P., Springel V., Hernquist L., 2013, *MNRAS*, 436, 3031

Vogelsberger M. et al., 2014, *MNRAS*, 444, 1518

Welker C., Devriendt J., Dubois Y., Pichon C., Peirani S., 2014, *MNRAS*, 445, L46

White S. D. M., 1979, *ApJ*, 229, L9

APPENDIX A: COMPARISON OF METHODS FOR CLASSIFYING ELLIPTICALS

We use the κ parameter (equation 1), as detailed in S+12, to separate the populations of spiral and elliptical galaxies based on their kinematics. While it performs well for high-mass galaxies, well matching observations (Conselice 2006) below $M_* \approx 10^{10.5} M_\odot$, it finds an unrealistically high population of bulge-dominated galaxies.

Optical examination of a handful of these galaxies still shows strong disc-like features down to $\sim 10^{10} M_\odot$, but with a much more bulge-dominated structure than we would expect to see for most galaxies at this scale. Below this mass, it is hard to derive, by visual examination, clear structure or shape. Similar results were seen in Illustris by Snyder et al. (2015) and Rodriguez-Gomez et al.

(2017), where low-mass galaxies are bulge dominated by kinematic measures, but have SFRs and disc properties characteristic of spiral galaxies. Dividing the population of galaxies by morphology gives a population of spirals and ellipticals that better fits with observational data, even at low mass ranges. Thus, we also explore a range of other metrics by which to separate spirals and ellipticals.

S+12 suggest a second method to determine the degree of rotation of a galaxy, and therefore determine if it is a spiral or an elliptical galaxy that we test here to compare its predictions and justify our chosen methods.

The authors use the distribution of the *circularity* parameter, $\epsilon_i = j_{z,i}/j_{c,i}(E_i)$, for each star particle's orbit. We define $j_{c,i}(E_i)$ as the angular momentum of a star on the circular orbit that shares the same binding energy, $E_i = K_i + \Phi(r_i)$.

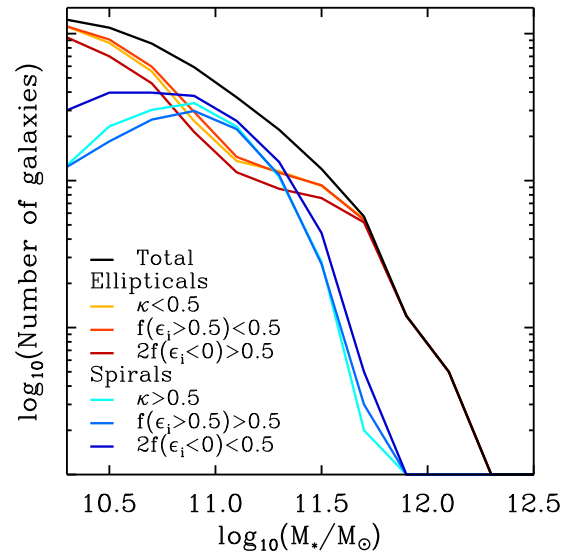


Figure A1. Stellar mass function of Illustris galaxies, separated by galaxy type based on three different measures of galaxy morphology (see the text). The κ parameter is the measure we use to separate spirals and ellipticals throughout the rest of our analysis. It can be seen that it agrees well with the other methods tested.

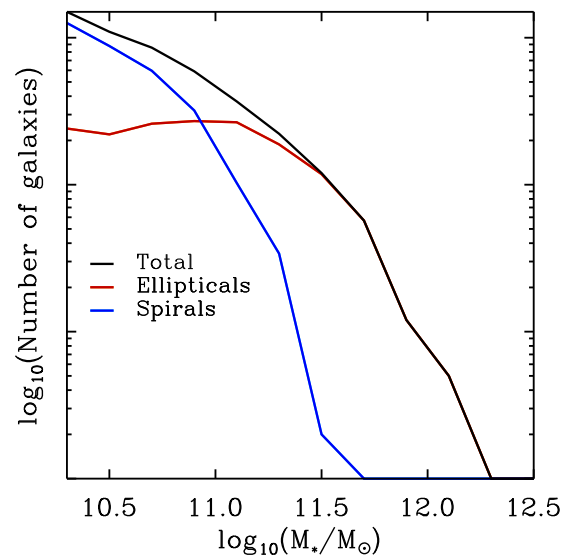


Figure A2. Similar to Fig. A1, but here galaxies are split based on the cutoff in $g - r$ band luminosity from equation (A1).

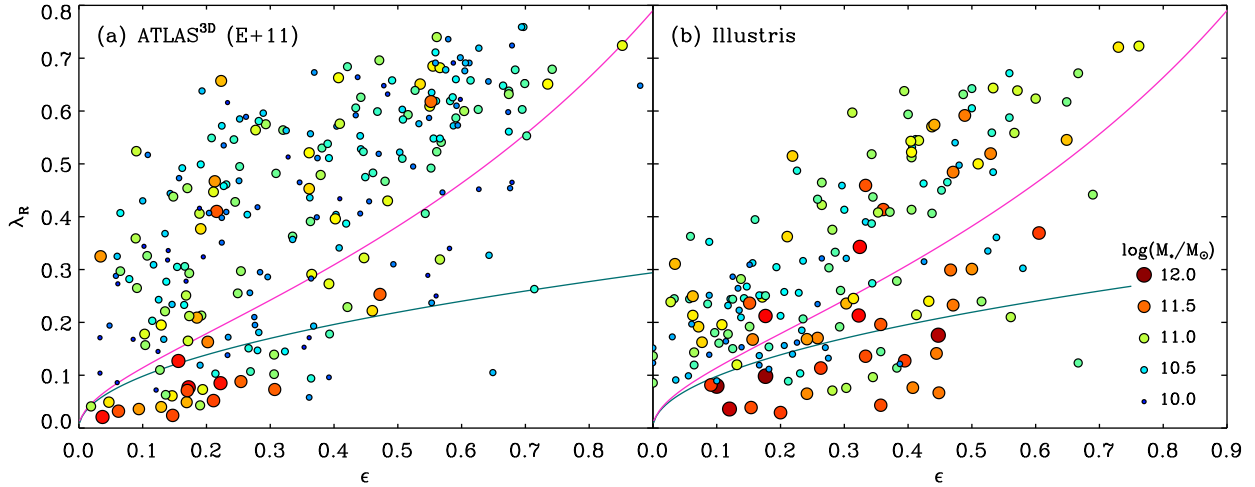


Figure A3. Distribution of ETGs in the ϵ - λ_R plane, as in Fig. 3, but using $g - r$ luminosity, rather than κ as the cutoff between spirals and ellipticals. We find a smaller number of ellipticals by the same selection criteria, roughly half those in the ATLAS^{3D} survey, and a similar distribution, with a slightly higher fraction of highly elongated or fast-spinning galaxies compared to that found with a κ cutoff.

This is a measure of how close each star particle is to a circular orbit, as we would expect in the disc of a spiral galaxy with ϵ_i has a maximum value of 1. For an orbit completely out of alignment with the galaxy’s total angular momentum, or with a very eccentric orbit, as we might expect in the bulge or in an elliptical galaxy ϵ_i will tend to 0.

Hence, by binning star particles by radius and averaging over their individual potentials, we find the circular radius r_c such that the energy of the star particle

$$E_i = K_{c,i} + \Phi(r_{c,i}) = -r_{c,i} \left. \frac{d\Phi}{dr} \right|_{r_{c,i}} + \Phi(r_{c,i})$$

which we then use to find $j_{c,i} = m_i r_{c,i} v_{c,i}(r_{c,i})$.

If we look at the distribution of ϵ_i for all stars in the galaxy, we see clear distinctions between bulge- and disc-dominated galaxies. To then classify galaxies as spirals or ellipticals, we quantify the number of stars in the bulge and the disc (this is approximately equal to the mass of stars in each as every star particle in Illustris has similar mass). We look at two different measures, $f(\epsilon > 0.5)$, the fraction of stars with ϵ_i greater than 0.5, i.e. the fraction of the stars in the disc, and $1 - 2f(\epsilon < 0)$, which quantifies the fraction of stars not in the bulge (relying on the fact that the distribution of stars in the bulge should be symmetrical around $\epsilon = 0$).

We take the cutoff for both of these measures to be the same as for κ . For $f(\epsilon > 0.5)$ or $1 - 2f(\epsilon < 0)$ greater than 0.5, we take the galaxy to be a spiral, and for values less than 0.5 we conclude that the galaxy is elliptical. In Fig. A1 is shown the stellar mass function, separated by type of galaxy as concluded by each method.

The three methods, whilst not in exact concurrence, are in good agreement. Thus, to separate spirals and ellipticals in our sample, we use the κ parameter, both because it gives the intermediate values for fraction of spirals and ellipticals, and because it is more reliable and less computationally expensive when computed for a very large number of galaxies.

We also present numerical results from our tests using $g - r$ band luminosity as the divide between spiral and elliptical galaxies, with a cut defined by equation (A1) (Figs A2 and A3).

We also experimented with making a cutoff between star-forming and quiescent galaxies based on their magnitude in the g and r bands. Galaxies for which $g - r$ is large are redder with little star

formation and these quiescent galaxies are often ellipticals, whilst smaller $g - r$ colours characterize bluer, star-forming galaxies, which in observational surveys correspond well with the population of spirals (Kormendy 2016).

We define a cut between star-forming galaxies as those below the line

$$\log_{10}(g - r) = 0.1 \log_{10}(M_*) - 0.5 \quad (\text{A1})$$

and quiescent galaxies as those above, motivated by the distribution of the whole sample of galaxies in Illustris (Vogelsberger et al. 2014). The luminosities are found by summing the individual luminosity of all stellar particles in the galaxy. The fraction of quiescent to star-forming galaxies, by mass, is in line with observations (Muzzin et al. 2013) over the whole mass range examined (down to haloes with stellar mass of $\sim 10^{10} M_\odot$).

Fig. A3 is a comparison with the galaxy population found in the ATLAS^{3D} survey, as presented in Section 3.1 using a cutoff defined by κ . We find less galaxies classified as ellipticals in the same volume, roughly half the previous number, with a wider spread in the distribution. There are more, faster spinning galaxies included though still few as rapidly rotating as in the ATLAS^{3D} survey. The population of high-mass galaxies is essentially unchanged, still with particularly elongated high-mass SRs as mentioned in Section 3.1.

Fig. A2 shows the stellar mass function derived using a colour cut. Whilst the results are more in line with the observed stellar mass function at low masses, we believe that this is due to the dependence of both on galaxy mass, rather than any strong link between luminosity and kinematic behaviour. Bottrell et al. (2017) performed similar analysis on carefully constructed mock images of Illustris galaxies and found a persistent disagreement with kinematic and photometric measures of bulge and disk fractions at stellar masses lower than $10^{11} M_\odot$.

However, the $g - r$ band is sensitive to dust and to the radius out to which luminosity is measured. The $g - r$ luminosity is strongly dependent on the mass, as is the stellar mass function, and hence we see our $g - r$ classification giving the expected fractions of spirals and ellipticals. However, κ better represents the morphology and kinematics of the individual galaxies and it is the measure we use throughout the rest of this work.

APPENDIX B: FITTING ISODENSITY CONTOURS TO FIND BOXY AND DISCY ELLIPTICALS

We seek to expand the Fourier series of the residuals of a galaxy's isodensity contours (equation 7) to find the sign and magnitude of the a_4 coefficient. This tells us if the elliptical is boxy ($a_4 < 0$) or discy ($a_4 > 0$). The fitting is done by a non-linear least-squares fit using a Levenberg–Marquardt algorithm, giving equal weight to each residual.

For each galaxy, we perform this analysis for three contours with areas equal to 0.6, 0.8 and 1.0 times the area of projected half-mass area of the galaxy and average the results. An example of three such contours is shown in Fig. A4, from top to bottom we have a poorly resolved galaxy classified as a boxy elliptical, a clear boxy elliptical and a clear discy elliptical. The deviations from an ellipse are very slight and thus noise introduced by substructure in the halo, binning into pixels and random variations can lead to significant variation. The resolution needed to accurately measure a_4 is significantly higher than our cutoff for well-resolved galaxies, appearing to only be well suited for galaxies above $10^{11} M_{\odot}$ or higher.

APPENDIX C: CHARACTERIZING GALAXIES WITH A CONSTANT DEGREE OF ROTATIONAL SUPPORT

Here we reproduce the derivation, presented in Cappellari et al. (2007) and E+11, of an approximate relationship between λ_R and ϵ for galaxies with a constant degree of rotational support.

If the majority of stars are on circular orbits, i.e. a high degree of rotational support, we can predict, given the anisotropy of those orbits, the shape of the galaxy. Assuming some constant relation between the anisotropy (δ) and ϵ , $\delta = c\epsilon$, galaxies with a high degree of rotational support will have a high c (tending to 1) and those with more radial less ordered orbits will have c tending to 0.

Thus, we can compare FRs and SRs via their rotational support, over a range of ellipticities, by finding the form of the relationship

$\delta = c\epsilon$ for a given constant c and converting it into a relationship between ϵ and λ_R .

The global anisotropy parameter for an edge-on system (Binney 2005) is

$$\delta = 1 - \frac{1 + (V/\sigma)^2}{\Omega (1 - \alpha (V/\sigma))^2}, \quad (\text{C1})$$

where α is a dimensionless constant dependent on the density profile, taken as ~ 0.15 from comparison to isotropic models,

$$\left(\frac{V}{\sigma}\right)^2 = \frac{\langle V^2 \rangle}{\langle \sigma^2 \rangle}, \quad (\text{C2})$$

and Ω is a measure of the ratio of potential of the system in the plane of the galaxy compared to perpendicular to the plane and is given by

$$\Omega(e) = \frac{1}{2} \frac{\arcsin(e) - e\sqrt{1-e^2}}{e\sqrt{1-e^2} - (1-e^2)\arcsin(e)}, \quad (\text{C3})$$

where $e(\epsilon) = \sqrt{1 - (1 - \epsilon)^2}$ (Cappellari et al. 2007). Rearranging gives

$$\left(\frac{V}{\sigma}\right)^2 = \frac{\Omega(1 - \delta) - 1}{1 + \alpha\Omega(1 - \delta)}. \quad (\text{C4})$$

Finally, E+11 combine this with the relationship between (V/σ) and λ_R ,

$$\lambda_R \equiv \frac{\langle R|V| \rangle}{\langle R\sqrt{V^2 + \sigma^2} \rangle} \approx \frac{k(V/\sigma)}{\sqrt{1 + k^2(V/\sigma)^2}}, \quad (\text{C5})$$

where $k \approx 1.1$ is found to be in good agreement with observations and models.

Cappellari et al. (2007) found that a value of c , the constant of proportionality between ellipticity and anisotropy, of roughly 0.7 characterized FRs well.

This relationship is shown as the magenta line in Fig. 3 and a linear scaling of it is used to determine a cutoff between FRs and SRs for galaxies viewed edge-on (equation 6).

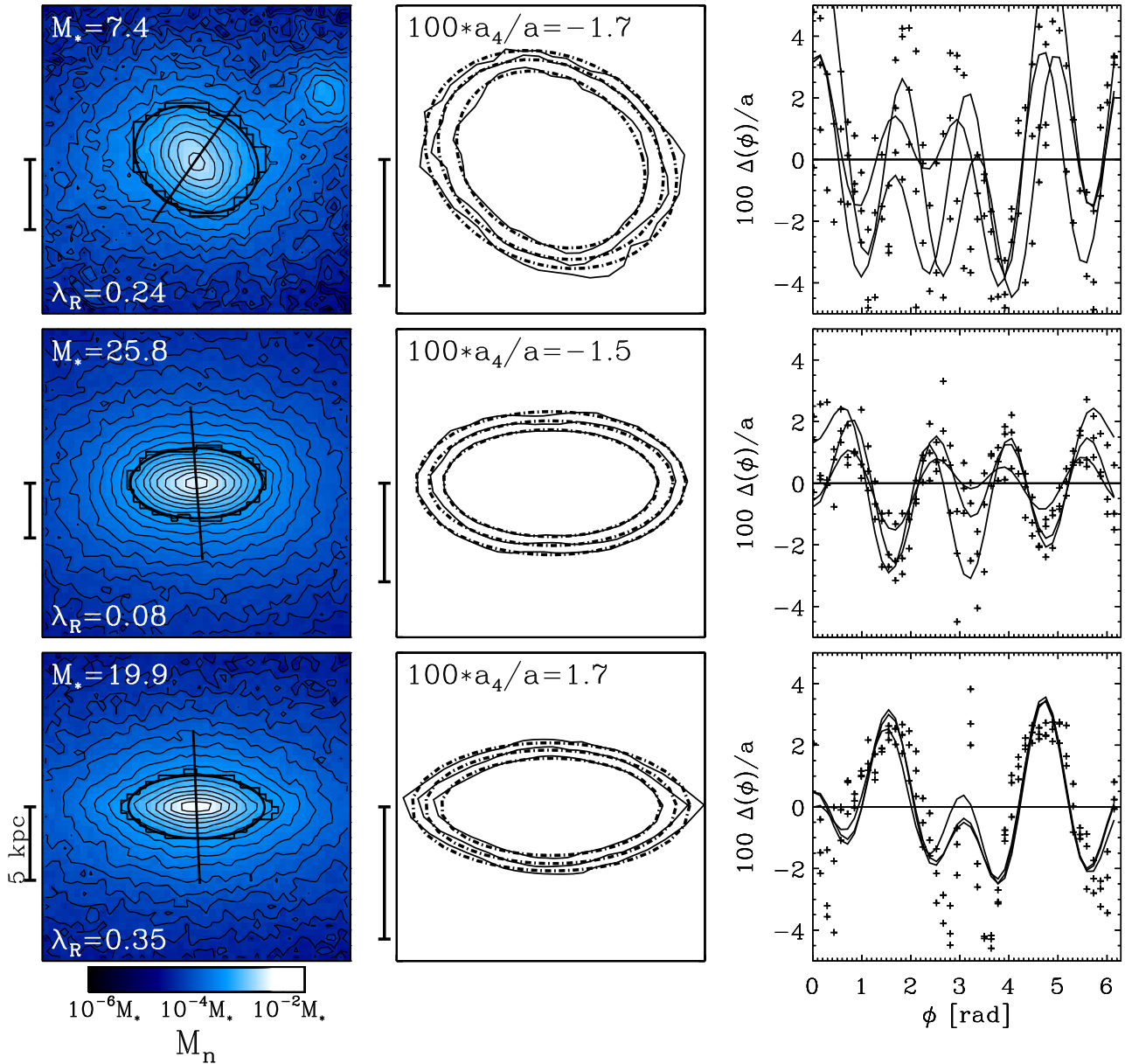


Figure A4. Measuring the a_4 parameter for three Illustris galaxies. On the left, we show projected stellar density (as in Fig. 1) with a number of isodensity contours, thin black lines, added. The next panel shows a magnified image of the isodensity contours, thin black line, and fitted ellipses, thick dashed line, for the half-mass contour and the contours with 0.6 and 0.8 times the area of the half-mass contour. The rightmost panel shows the residuals of the contour from the fitted ellipse, normalized by the major axis of each ellipse, as black crosses, and the fitted Fourier expansion, as a thin black line. All scale bars are 5 kpc in length.

This paper has been typeset from a $\text{\TeX}/\text{\LaTeX}$ file prepared by the author.